ISA Transactions 145 (2024) 330–354

Contents lists available at ScienceDirect

ISA Transactions

journal homepage: www.elsevier.com/locate/isatrans

Research article

Prescribed performance control of a robotic manipulator with unknown control gain and assigned settling time

Pooria Ghanooni [a], Hamed Habibi [b], Amirmehdi Yazdani [c,*], Hai Wang [c], Somaiyeh MahmoudZadeh [d,e], Antonella Ferrara [f]

[a] Department of Electrical Engineering, Azad University of Mashhad, Mashhad, Iran
[b] Interdisciplinary Centre for Security, Reliability and Trust, University of Luxembourg, L-1855 Luxembourg, Luxembourg
[c] School of Engineering and Energy, Murdoch University, Perth, WA 6150, Australia
[d] CCIT, UDST University, Doha, Qatar
[e] School of IT, Deakin University, Geelong, Australia
[f] Department of Electrical, Computer and Biomedical Engineering, University of Pavia, 27100 Pavia, Italy

ARTICLE INFO

Keywords:
Barrier lyapunov function
Constrained control
Prescribed performance bound
Robotic manipulator

ABSTRACT

This paper presents a control method for trajectory tracking of a robotic manipulator, subject to practical constraints and uncertainties. The proposed method is established upon an adaptive backstepping procedure incorporating a tangent-type barrier Lyapunov function and it preserves some important metrics of trajectory tracking such as fast and user-defined settling time response and robustness against actuation faults and unknown control gain. The proposed design maintains the system trajectory within a prescribed performance bound and relaxes the assumption of the bounded initial condition. These salient features preserve the system within a safety bound and, consequently, guarantee the system stability and safety. The performance of the proposed control method is validated on a 3-DOF PUMA 560 robotic manipulator benchmark model, with different operation scenarios. The simulation results confirm the effectiveness and robustness of the proposed control method.

1. Introduction

Prescribed performance control of a robotic manipulator, as a safety-critical system, is crucial in practical applications [1–3]. The human operator and the robotic manipulator might experience catastrophic risks if the system's states reach an unsafe region, or the system cannot deliver the expected performance [4]. In the robotic manipulators, this prescribed performance verification is tightly engaged with trajectory tracking control, where preserving performance metrics, e.g., fast transient response, finite-time convergence, and guaranteed stability is vital [5]. The importance of these performance metrics is demonstrable in practice (see [4,6] and references therein). However, as the robotic manipulator is a highly nonlinear system with uncertainties, the control system design is always challenging and demands innovative solutions. This means that imprecise knowledge of the manipulator kinematics in conjunction with the link flexibility, friction, and actuator backlash, should be carefully considered. There exist various methodologies to deal with the high-performance control of robotic manipulators. A common taxonomy encompasses methods like proportional-integral-derivative (PID) control [7], adaptive and learning-based control [2], sliding mode control (SMC) [1,8–10], inverse dynamics control [11], sampled-data control [12], homogeneous control [13], and optimal control [14].

Different complexities in the robotic manipulators, which are associated with unmodeled dynamics, unknown parameters, disturbances, and uncertainties, have motivated researchers to employ adaptive and learning-based control methods. This paves the way for the identification of the uncertain robotic manipulator systems and compensation for the impact of state constraints while the system stability is preserved. For instance, in [15], the finite-time tracking controller is designed within backstepping framework for uncertain multi-input–multioutput nonlinear systems (which can be a representation of a robotic manipulator system) with input backlash. The neural network (NN) is used to approximate the unknown dynamics. In [16], an adaptive fuzzy NN impedance control for a constrained robotic manipulator is designed, using logarithm barrier Lyapunov function (BLF). The NN is designed to

* Corresponding author.
E-mail address: Amirmehdi.Yazdani@murdoch.edu.au (A. Yazdani).

https://doi.org/10.1016/j.isatra.2023.12.011
Received 20 June 2022; Received in revised form 25 September 2023; Accepted 6 December 2023
Available online 13 December 2023

estimate unknown system dynamics. Also, an observer is designed to estimate disturbance. In [17], an adaptive NN-based strategy is proposed to control a robotic manipulator with unknown backlash. In [6], adaptive NNs are employed to approximate the robotic manipulator dynamics with input dead zone and output constraint, utilizing a BLF. In [18], NNs are utilized for the robotic manipulator control subject to model uncertainties and frictional forces. In [19], radial basis function NN is used for adaptive impedance control of a robotic manipulator subject to input saturation and in [20], Fourier series expansion is used in a learning based scheme with guaranteed output constraint. In [21], an adaptive fuzzy NN control is used to control a 3-DOF robotic manipulator with unknown dynamics and constraints on states. However, the major challenge with these controllers is the computational complexity associated with training processes which makes them not suitable for real-time implementation. Therefore, the need for an easy-implementable, robust, and tractable control is inevitable.

In this regard, robust control techniques have shown significant characteristics in fault and disturbance rejection when dealing with strong nonlinearity and uncertainty. However, the classic SMC techniques often suffer from chattering phenomenon, and requires a priori knowledge of the upper bound of uncertainties, faults, and disturbances. To address these drawbacks, advanced SMC techniques such as higher-order SMC and terminal SMC have been proposed [22]. The initial ground-breaking research in this regard includes robust terminal SMC [23] for finite-time tracking [24,25]. However, the major drawback with the proposed terminal SMC is the singularity phenomenon [26]. This restricts the practical applications of the terminal SMC and negatively impacts the control performance. The singularity problem of the terminal SMC can be addressed by introducing a new sliding surface that provides non-singular finite-time tracking performance [27]. To compensate for the steady-state error and improving the finite-time convergence without increasing the sample time and bandwidth, an integral fast terminal SMC has been proposed in [28]. However, the convergence rate highly depends on the initial conditions, representing the possibility of unbounded growth of convergence time while the initial conditions are far beyond the equilibrium region.

Recently, higher-order SMC methods have been employed for finite-time stable control of robotic manipulators. In [1], an adaptive high-order terminal SMC is developed to obtain robust and finite-time convergence control of a robotic manipulator with backlash hysteresis. In addition, an adaptive mechanism is developed to compensate for unknown dynamics. The performance of the proposed high-order terminal SMC against a benchmark 3-DOF PUMA 560 robotic manipulator is evaluated through simulation and the results confirm the finite-time stability and high tracking outcome. However, the control signal still suffers from the chattering phenomenon under noise impact and dependence of system performance to the initial conditions remains unaddressed. In [4], an integral non-singular fast terminal SMC is employed to address the robust fault-tolerant control of robotic manipulators. The proposed control strategy features finite-time convergence as well as stability. On top of that, an adaptive mechanism is designed to overcome the controller dependence to the prior knowledge of uncertainty bound. The simulation study, applied on the 3-DOF PUMA 560 robotic manipulator model, demonstrates the performance effectiveness of this control strategy, even in presence of actuator faults. However, the controller cannot simultaneously preserve robustness and fast convergence, and it requires a mechanism for fine-tuning the controller parameters. In [29], a backstepping based adaptive finite-time tracking control is proposed for uncertain robotic manipulators with unknown backlash. The proposed control strategy accommodates the explosion of the complexity of conventional backstepping design and the issue of finite-time convergence. The performance of the proposed controller on a simplified 2-DOF model of PUMA 560 robotic manipulator shows the finite-time position tracking error convergence even in presence of unknown backlash. However, the major drawback is that the convergence time highly depends on the initial conditions and cannot be predefined. As a result, the initial conditions affect the controller finite-time performance.

In the preceding works, the control performance is subject to some critical assumptions on the linearity-in-parameters associated with the uncertainty, pre-set initial conditions and bounds, and extremely impractical large bound for the manipulator system. In addition, the required cumbersome training process of the existing fuzzy- or NN-based solutions for unmodeled dynamics and uncertainty approximation is neither computationally efficient nor feasible for controller implementation in real-world applications. In practice, the manipulator system often experiences practical constraints such as backlash hysteresis, actuator faults, and model uncertainty and thus the control mechanism should be able *to simultaneously preserve the control objectives* of high tracking precision, user-defined settling time, handling of arbitrary initial conditions, and chattering-free control signal, as well as maintaining the asymptotically stability and safety region of the manipulator system. However, there exists lack of research on developing such a universal control system in the literature.

Motivated by the above-mentioned issues and the existing gaps, this paper proposes a robust high precision control methodology with guaranteed prescribed tracking performance for a robotic manipulator system. The proposed control method uses the principles of adaptive backstepping procedure and tangent-type BLF to maintain the states within the prescribed performance bound (PPB). The effect of arbitrary initial conditions is compensated by incorporating a scaling function with a user-defined settling time. Thus, the assumption of the bounded initial conditions is relaxed. Moreover, the proposed method complies with the practical constraints associated with robotic manipulator systems and hence very large performance bounds are avoided. The designed control scheme compensates for the faults, backlash, disturbance, and unknown control gain effects, to guarantee safe and reliable operation. In Table 1, a comparative literature review is given to further highlight the motivation and novelties of the proposed control.

Accordingly, the main contributions of this paper can be summarized as follows:

1) The proposed design guarantees the closed-loop stability (theoretically proven) in presence of disturbances, actuation faults, backlash, and uncertainty. Moreover, it can satisfy the prescribed tracking performance by delivering high precision and fast response to a vast range of the desired trajectories.
2) Compared to [20,32–36], the proposed controller is robust against unmodeled dynamics and capable to handle the unknown control gain. This stems from the fact that the control distribution matrix is the inverse of the inertia matrix, which itself is a function of angular positions, thus, time-varying. In addition, the inertia matrix might change due to unforeseen model uncertainty.
3) Compared to [18–21,32–35], in this work, the use of computationally expensive function approximators is avoided, and thus the real-time implementation of the proposed method in practice is achievable. This is made via the incorporation of a computable core function with an unknown scalar gain.
4) Compared to [32,34,35], the proposed design provides a user-defined settling time to tackle the arbitrary initial conditions. This provides a significant advantage to simply adjust the rising speed of the system and to avoid a large bound which is not suitable for practical use of manipulator systems.
5) In contrast to the reported works of the literature [22,27], the control signal generated in this work is continuous which is more suitable for practical applications given the electromechanical nature of robot manipulators.

The remainder of this paper is arranged as follows. The system description and technical preliminaries are discussed in Section II. Section III provides the control design procedure, addressing its salient features, with stability analysis. In Section IV, the performance of the

Table 1
Comparative literature review (NA denotes Not Applicable).

Method	Paper	Benefits								
		Robustness	Chattering free	Predefined settling time	Use of neural networks	Backlash handling	Safety bound	Fault tolerance	Arbitrary initial condition	Unknown control gain
PID	[30]	No	NA	No	No	No	No	No	No	Yes
Adaptive backstepping learning-based control NN and fuzzy	[31]	Yes	Yes	Yes	No	Yes	No	No	No	No
	[2,6, 17–19, 21, 32–35]	Yes	NA	No	Yes	Yes	Yes	No	No	No
SMC	[1,8,9, 26]	Yes	No	No	No	Yes	No	Yes	No	No
Terminal SMC	[1,4,22, 27]	Yes	Yes	No	No	Yes	No	Yes	No	No
Integral SMC	[28]	Yes	Yes	Yes	No	Yes	No	Yes	No	No
Inverse dynamics control	[11]	No	NA	No	No	No	No	No	NA	No
Homogeneous control	[13]	Yes	Yes	Yes	No	No	No	No	No	No
Optimal control	[14]	No	NA	No	No	No	Yes	No	Yes	Yes
PPB based control	[21, 32–35]	Yes	NA	No	Yes	Yes	Yes	Yes	No	No
Proposed Control		Yes	Yes	Yes	No	Yes	Yes	Yes	Yes	Yes

proposed design is studied through extensive numerical simulations. Finally, Section V concludes the paper.

2. System description and technical preliminaries

2.1. Robotic manipulator model and control objective

Consider the robotic manipulator dynamics as

$$\ddot{q} = M^{-1}(q)(u_a(t) - H(q,\dot{q})\dot{q} - F(\dot{q}) - G(q) - \tau_d(t)\,), \tag{1}$$

where $q \in \mathbb{R}^n$, $u_a \in \mathbb{R}^n$, $M(q) \in \mathbb{R}^{n\times n}$, and $H(q,\dot{q}) \in \mathbb{R}^{n\times n}$ represent the positions, actuator input, positive definite inertia matrix, and Coriolis/centripetal forces, respectively. Also, $F(\dot{q}) \in \mathbb{R}^n$, $G(q) \in \mathbb{R}^n$, and $\tau_d \in \mathbb{R}^n$ are the friction force, the gravity force and the unknown disturbance, respectively. This disturbance can represent the bounded external perturbation and system uncertainty. Due to the fast actuator response, the actuator is modelled as [4]:

$$u_a(t) = \Gamma_1(t)u(t) + \Gamma_2(t), \tag{2}$$

where $u(t) \in \mathbb{R}^n$ is control signal commanded by the controller, $\Gamma_1(t) = diag\{\gamma_{1,1}(t - t_{f_{1,1}}), \ldots, \gamma_{n,1}(t - t_{f_{n,1}})\} \in \mathbb{R}^{n\times n}$ is the actuator effectiveness diagonal matrix, $\Gamma_2(t) = \left[\gamma_{1,2}\left(t, t_{f1,2}\right), \ldots, \gamma_{n,2}\left(t, t_{fn,2}\right)\right]^T \in \mathbb{R}^n$ is the actuator additive bias. In this paper, it is assumed that the actuator dynamics are fast enough, compared to the dynamics of the robot. Therefore, we could assume that the actuator effort on the dynamics is the commanded control input, i.e., $u_a(t) = u(t)$, where $u_a \in \mathbb{R}^n$ is actuator input and $u(t) \in \mathbb{R}^n$ is a control signal commanded by the controller [4,37]. However, due to the actuator malfunction, there might be some bias in the actuator model, which is modelled as $\Gamma_2(t)$ in (2). On the other hand, over a long period of operation, the actuator might lose its effectiveness by less than 100%. This is modelled as $\Gamma_1(t)$ in (2) [38]. When the actuator is fault-free, then $\Gamma_1 = I_n$ and $\Gamma_2 = 0_{n\times 1}$. On the other hand, the actuator effectiveness $\Gamma_1(t)$ can represent the multiplicative faults. For this aim and to cover a family of abrupt and incipient faults,

$$\gamma_{i,1}\left(t - t_{f_{i,1}}\right) = \begin{cases} 1, t < t_{f_{i,1}} \\ 1 - b_i\left(1 - e^{a_i\left(t_{f_{i,1}} - t\right)}\right), t \geq t_{f_{i,1}} \end{cases}, \tag{3}$$

where $t_{f_{i,1}}$ is the moment i^{th} actuator starts losing its full effectiveness, $0 \leq b_i < 1$ is the percentage of effectiveness lost, and $a_i \in \mathbb{R}_{>0}$ is the evolution rate. For incipient faults a_i is small and for abrupt faults a_i is large. It should be noted that $t_{f_{i,1}}$, b_i and a_i are unknown constants. It is worth noting that, $0 < \gamma_{i,1}\left(t - t_{f_{i,1}}\right) \leq 1$ for $i = 1, \ldots, n$. Also, Γ_1 is a positive definite matrix. On the other hand, $\gamma_{i,2}\left(t, t_{f_{i,2}}\right) \in \mathbb{R}$ is a time variable unknown function applied at the moment $t_{f_{i,2}}$. For $t < t_{f_{i,2}}$, $\gamma_{i,2}\left(t, t_{f_{i,2}}\right) = 0$. Accordingly, the state-space model of the robotic manipulator can be obtained as,

$$\begin{aligned} \dot{x}_1 &= x_2, \\ \dot{x}_2 &= f(q,\dot{q}) + g(q)\Gamma_1(t)u + d(q,t), \end{aligned} \tag{4}$$

where $x_1 = q$, $x_2 = \dot{q}, f(q,\dot{q}) = -M^{-1}(q)H(q,\dot{q})\dot{q} - M^{-1}(q)G(q)$, $g(q) = M^{-1}(q)$ and $d(q,t) = M^{-1}(q)\Gamma_2(t) - M^{-1}(q)\tau_d(t) - M^{-1}(q)F(\dot{q})$. The robotic dynamics (1) satisfies the following standard property as:

$$0 < \underline{M} = \lambda_m(M(q)\,) \leq \|M(q)\,\| \leq \lambda_M(M(q)\,) = \overline{M}, \tag{5}$$

where $\lambda_m(X)$ and $\lambda_M(X)$ represent the minimum and maximum eigenvalues of X, respectively. As M is positive-definite, then $\rho(M) \subset \mathbb{R}_{>0}$, where $\rho(M)$ is the spectrum of matrix M. Therefore, M is invertible. Consequently, it is easy to obtain that $g(q)$ is positive definite and

$$0 < \underline{g} \leq \|g(q)\,\| \leq \overline{g}, \tag{6}$$

where $\underline{g} = \overline{M}^{-1}$ and $\overline{g} = \underline{M}^{-1}$.

Assumption 1 [4]: The unknown disturbance $\tau_d(t)$ and frictional force $F(\dot{q})$ are assumed to be upper bounded. Also, due to the bounded range of actuator effort, $\gamma_{i,2}\left(t, t_{f_{i,2}}\right)$ is bounded as $\left|\gamma_{i,2}\left(t, t_{f_{i,2}}\right)\right| \leq \overline{\gamma}_{i,2}$, for $i = 1,\ldots,n$, where $\overline{\gamma}_{i,2}$ is an unknown positive constant. Accordingly, this yields that $d(.)$ is upper bounded as $\|d(.)\| \leq \overline{d}$, where $\overline{d}$ is an unknown positive constant. Also, the desired trajectory $x_d \in \mathbb{R}^n$, its first- and second-time derivatives are known and bounded.

Remark 1: In similar works [33–35], the control gain g is assumed to be known a priori. However, as g is time variable and there may be some modelling uncertainties, this assumption is not satisfied. In this paper, we relax this restrictive assumption, using the Nussbaum type function. Furthermore, in some works, [24], the motor dynamics is also considered. However, in this work, we only consider the manipulator

dynamics, as it's the dominant dynamics of the closed-loop system. More importantly, the presented results can be extended to such cases considering the motor dynamics.

The main objective of this paper is to design the control u to steer x_1 towards the desired trajectory $x_d \in \mathbb{R}^n$ and to keep the corresponding tracking error within a given PPB. This should encompass arbitrary initial conditions with preassigned settling time in the presence of actuator faults, backlash, disturbance and model uncertainty. Furthermore, the control gain is assumed to be unknown.

2.2. Crude information of the model

The lumped nonlinear term $f(q,\dot{q})$ is not accurately computable as it includes the Coriolis, centripetal and friction forces. Also, it includes the inertia matrix M which often varies during the operation. Accordingly, in this paper, it is assumed that only some crude structural information on the nonlinear term is extractable. This relates to the extraction of the deep-rooted information from the nonlinearities of the system, which can be readily obtained for practical systems [39]. This can be formulated as an upper bound on the nonlinear term, including a computable core function with an unknown scalar gain. This relaxes the need for the accurate estimation of the nonlinearity via computationally expensive schemes such as NN or fuzzy systems. Considering the robotic system structure, we can extract the information from the nonlinear function $f(q,\dot{q})$, as the following inequality,

$$\|f(q,\dot{q})\| \le a_0\varphi_0(q,\dot{q}), \tag{7}$$

where $\varphi_0(q,\dot{q}) = \|\dot{q}\|^2 + \|\dot{q}\| + 1$ is a nonnegative computable core function and a_0 is an unknown positive constant [39]. Accordingly, it is readily shown that

$$\|f(q,\dot{q}) + d(q,t)\| \le a\varphi(q,\dot{q}), \tag{8}$$

where $a = \max\{a_0, \bar{d}\}$ is an unknown positive constant and $\varphi(q,\dot{q}) = \varphi_0(q,\dot{q}) + 1$.

Remark 2: In some works, e.g., [32,33,35], the NN has been utilized to estimate the nonlinear function $f(q,\dot{q})$,leading to a numerically complex algorithm that is hard to be implemented in practice. The computational burden of NN grows with the number of inputs and the corresponding number of basis function centers. In contrast, in this paper, we have taken advantage of the useful information from the robotic system dynamic, which is encapsulated in $\varphi_0(q,\dot{q})$. Consequently, we only need to estimate the upper bound of scalar a_0, which is numerically inexpensive, compared to NN.

2.3. Scaling function

In this paper, to tackle arbitrary initial conditions, any non-zero and finite initial values are initially transferred to zero. Then after the settling time T_s is passed, the deferred constraints are imposed on the original states. In this manner, the restrictive assumptions on the initial values, given in [33–35], are relaxed. Also, there is no need for asymmetric time variable bounds with higher computational complexity. Based on the desirable performance, the settling time is defined by the user. To achieve this, the scaling function (9) is incorporated into the controller design:

$$\Phi(t) = \begin{cases} 1 - \left(\dfrac{T_s - t}{T_s}\right)^{\bar{n}+\nu}, 0 \le t < T_s \\ 1, T_s \le t \end{cases} \tag{9}$$

where $\bar{n}$ is the system order. Considering the dynamics (2), $\bar{n} = 2$. Also, T_s is user-defined settling time and $\nu \ge 2$ is a design parameter. It is worth noting that, the parameter ν can impose the desirable speed during the transient period. This design parameter gives freedom to adjust the rising speed, i.e., from scaled signal to actual signal, without reducing T_s. This is due to the fact that the settling time T_s is limited by the signal processing and communication time $\bar{T}_s$, i.e., $T_s \le \bar{T}_s$.

2.4. Technical preliminaries

The following definitions and lemmas are briefly recalled, which are used in the sequel.

Definition 1. Let $V(x(t))$ be a positive definite continuous and $x(t)$ is the solution of $\dot{x} = f(x)$ on an open region $\mathscr{O}$ with the boundary of $\partial\mathscr{O}$. If $\lim_{x\to\partial\mathscr{O}} V(x) = \infty$, then $V(x(t))$ is a BLF with continuous first-order partial derivatives within $\mathscr{O}$ excluding $\partial\mathscr{O}$, i.e., $\mathscr{O}\partial\mathscr{O}$. Consequently, $V(x(t)) \le \mathscr{V}$, $\forall t \ge t_0$ holds along the solution of $\dot{x} = f(x)$ for $x(t_0) \in \mathscr{O}\partial\mathscr{O}$, and some positive constant $\mathscr{V}$.

Definition 2. $x(t)$ is uniformly ultimately bounded (UUB) if there exists $T^*(k, x(t_0))$, with $k > 0$ such that for any compact set Ω and all $x(t_0) \in \Omega$, $\|x(t)\| \le k$, for $t \ge t_0 + T^*$.

Definition 3. Let the continuous function $N(x) : \mathbb{R}\to\mathbb{R}$ satisfies $\liminf_{x\to\infty} \int_{x_0}^{x} N(\tau)d\tau = -\infty$ and $\limsup_{x\to\infty} \int_{x_0}^{x} N(\tau)d\tau = +\infty$, for $x_0 \in \mathbb{R}$. Then, $N(x)$ is a Nussbaum-type function.

Lemma 1. The scaling function $\Phi(t)$, defined in (9), has the following useful properties.

i) As $\lim_{t\to T_s^-} \Phi(t) = \lim_{t\to T_s^+} \Phi(t) = 1$, then the scaling function is continuous for all $0 \le t$.

ii) As $\Phi(0) = 0$ and $0 < \Phi(t) < 1$ for $0 \le t < T_s$, then $\Phi(t) \in [0,1]$ for all $0 \le t$. Therefore, $\Phi(t)$ is bounded.

iii) $\Phi^{(i)}(t) = \begin{cases} \dfrac{(-1)^{i+1}(\bar{n}+\nu)!(T_s - t)^{\bar{n}+\nu-i}}{(\bar{n}+\nu-i)!T_s^{\bar{n}+\nu}}, 0 \le t < T_s \\ 0, T_s \le t \end{cases}$, for $i = 1, \ldots,$ $\bar{n}+\nu-1$, hence, $\Phi^{(i)}(0) = \frac{(-1)^{i+1}(\bar{n}+\nu)!}{(\bar{n}+\nu-i)!T_s^i}$ and $\lim_{t\to T_s^-} \Phi^{(i)}(t) = \lim_{t\to T_s^+} \Phi^{(i)}(t) = 0$. Therefore, $\Phi^{(i)}(t)$ is continuous up to order $\bar{n}+\nu-i-1$ and bounded for $0 \le t$.

iv) For $0 \le t < T_s$, $\dot{\Phi}(t) = (\frac{\bar{n}+\nu}{T_s})(1 - \frac{t}{T_s})^{\bar{n}+\nu-1}$, and therefore, $0 < \dot{\Phi}(t)$. Accordingly, $\Phi(t)$ is a strictly increasing function starting from $\Phi(0) = 0$ to $\Phi(T_s) = 1$, for$0 \le t < T_s$, and stays at its maximum $\Phi(t) = 1$ for all $T_s \le t$.

The proof of this is straightforward and therefore omitted.

***Lemma* 2.** [40] for any vectors $x,y \in R^n$, Cauchy-Schwarz Inequality is as $x^Ty \le ||x||||y||$. Then the following inequalities hold.

$$x^Ty \le ||x||||y|| \le ||x||^2||y||^2 + \frac{1}{4},$$

$$x^Ty \le ||x||||y|| \le \frac{||x||^2}{2} + \frac{||y||^2}{2}.$$

***Lemma* 3.** [7]: For any vector $x(t) \in \Theta$, where $\Theta = \{x(t) \in \mathbb{R}^n | \|x(t)\| < 1\}$ is a compact set, $\tan(\pi x^Tx/2) \le \pi x^Tx\sec^2(\pi x^Tx/2)$ holds true.

***Lemma* 4.** [7]: Let $V(t) > 0$ and $\omega(t)$ be smooth functions on $[0t_f)$. Also, $N(\omega(t))$ is a Nussbaum type function. If $V(t) < c_0 + \exp(-c_1t)\int_0^t (\Lambda(\tau)N(\omega(\tau)) + 1)\dot{\omega}\exp(c_1\tau)d\tau$ for any $t \in [0t_f)$, with positive constants c_0 and c_1, and $\Lambda(\tau)$ takes values in the unknown closed intervals $\mathscr{L} \in [r^+, r^-]$ with $0 \notin \mathscr{L}$, then $V(t)$, $\omega(t)$ and $\int_0^t \Lambda(\tau)N(\omega(\tau))\dot{\omega}\exp(c_1\tau)d\tau$ must be bounded on $[0t_f)$.

***Lemma* 5.** [39]: Let $X \in \mathbb{R}^{n\times n}$ be a symmetric matrix. For any nonzero vector $x \in \mathbb{R}^n$ there is at least one eigenvalue of X in $(-\infty, x_0]$ and at least one in $[x_0, +\infty)$, for $x_0 = x^TXx/x^Tx$.

Hereafter, to simplify the subsequent notation, if there is no confusion, function arguments are omitted.

3. Main result

3.1. Control design

To initiate the design, we define the tracking errors as,

$$e_1 = x_1 - x_d, \tag{10}$$

$$e_2 = x_2 - \alpha_1, \tag{11}$$

where α_1 is virtual controller, designed later. Also, the scaled tracking error is obtained as

$$z_1 = \Phi e_1. \tag{12}$$

Considering the definition of $\Phi(t)$ in (9), the tracking error $e_1(t)$, with an arbitrary finite initial value, is transferred into the scaled tracking error $z_1(t)$, with the initial value $z_1(0) = 0$. On the other hand, $z_1(t)$ recovers the original tracking error $e_1(t)$ for $T_s \leq t$. With this feature, the problem of arbitrary initial condition in the context of BLF-based constrained control is resolved, as investigated in the sequel. The virtual control α_1 is designed as

$$\alpha_1 = \dot{x}_d - \Lambda_1 e_1, \tag{13}$$

where $\Lambda_1 = k_1 + \left(0.5\Phi^2 + \dot{\Phi}^2\|e_1\|^2\right)\sec^2(\chi_1) \in \mathbb{R}_{>0}$, $\chi_1 = 0.5\pi z_1^T z_1/\gamma_1^2$ and k_1 is a positive design parameter. Also, γ_1 is the selected bound imposed on the scaled tracking error $\|z_1\|$. Now, the proposed control u is designed as:

$$u = H()\alpha_2, \tag{14}$$

with the gain $H()$. The virtual control α_2 designed as

$$\alpha_2 = \Lambda_2 e_2, \tag{15}$$

where $\Lambda_2 = 0.5\widehat{\kappa}\varphi^2 + 0.5\|\alpha_1\|^2 + k_2$, and k_2 is a positive design parameter. Also, $\widehat{\kappa}$ is updated with the adaptive law

$$\dot{\widehat{\kappa}} = 0.5e_2^T e_2 \varphi^2 - \sigma\widehat{\kappa}, \widehat{\kappa}(0) > 0 \tag{16}$$

with positive design parameter σ. It is worth noting that $\widehat{\kappa}$ is the estimation of $\kappa = a^2$, which is an unknown positive constant. In this scheme the adaptive law (16) is only required, despite the NNs with a large number of adaptive laws.

The analytical solution of (16) is $\widehat{\kappa}(t) = \exp(-\sigma t)\widehat{\kappa}(0) + 0.5\int_0^t \exp(\sigma(\tau - t))e_2^T e_2 \varphi^2 dt$. Therefore, by selecting a positive initial condition for $\widehat{\kappa}$, i.e., $\widehat{\kappa}(0) \in \mathbb{R}_{>0}$, one can conclude that $\widehat{\kappa}(t)$ remains positive as an estimation of the positive constant κ. This further yields that $\Lambda_2 \in \mathbb{R}_{>0}$. Furthermore, in (15) $\dot{\alpha}_1$ is the time derivative of α_1 which is analytically computable as

$$\dot{\alpha}_1 = \ddot{x}_d - \Lambda_1 \dot{e}_1 - \Lambda_3 e_1, \tag{17}$$

with $\Lambda_3 = (\Phi\dot{\Phi} + 2\dot{\Phi}\ddot{\Phi}\|e_1\|^2 + 2\dot{\Phi}^2 e_1^T \dot{e}_1)\sec^2(\chi_1) + 2\pi(0.5\Phi^2 + \dot{\Phi}^2\|e_1\|^2)\sec^2(\chi_1)\tan(\chi_1)(z_1^T\dot{z}_1)/\gamma_1^2 \in \mathbb{R}$.

The first-time derivative of z_1 is obtained as

$$\dot{z}_1 = \dot{\Phi}e_1 + \Phi\dot{e}_1 = \dot{\Phi}e_1 + \Phi(e_2 + \alpha_1 - \dot{x}_d). \tag{18}$$

The control gain $H()$ is yet to be designed. In some works, e.g., [33–35], the inertia matrix is assumed to be known, and accordingly $H() = -g^{-1}(q)$. However, this assumption may be violated in the presence of uncertainty in the inertia. Therefore, in this paper, this assumption is relaxed with the aid of the Nussbaum type function. Accordingly, the control gain is designed as

$$H() = N(\xi), \tag{19}$$

where $N(\xi) \in \mathbb{R}$ is a Nussbaum type function and ξ is an intermediate variable and updated as

$$\dot{\xi} = e_2^T \alpha_2. \tag{20}$$

It is evident that neither the design control u nor the control gain $H()$ is a function of $g(q)$.

3.2. Stability analysis

We first focus on the fault-free case, i.e., $\Gamma_1 = I_n$ and $\Gamma_2 = 0_{n\times 1}$. The fault-tolerance properties are discussed later. To analyze the stability of the closed-loop system and to address the constraint on e_1, a BLF is constructed as

$$V_1 = \frac{\gamma_1^2}{\pi}\tan(\chi_1). \tag{21}$$

It is readily shown that V_1 is positive definite and well defined in the set $\Omega_1 = \{z_1 \in \mathbb{R}^n | \|z_1\| < \gamma_1\}$. Equivalently, it can be stated that in the set Ω_1, $z_1^T z_1/\gamma_1^2 < 1$. Using $\dot{z}_1$ given in (18), the first-time derivative of V_1 is obtained as

$$\dot{V}_1 = \sec^2(\chi_1) z_1^T \dot{z}_1 = \sec^2(\chi_1) z_1^T(\dot{\Phi}e_1 + \Phi e_2 + \Phi\alpha_1 - \Phi\dot{x}_d). \tag{22}$$

By using Lemma 2, one can obtain that

$$\sec^2(\chi_1) z_1^T \dot{\Phi} e_1 \leq \|z_1\|^2 \sec^4(\chi_1)\dot{\Phi}^2\|e_1\|^2 + \frac{1}{4}, \tag{23}$$

$$\sec^2(\chi_1) z_1^T \Phi e_2 \leq \frac{\|z_1\|^2 \sec^4(\chi_1)\Phi^2}{2} + \frac{\|e_2\|^2}{2}. \tag{24}$$

By using (23), (24) and the virtual control α_1 (13), (22) yields

$$\dot{V}_1 \leq -k_1\|z_1\|^2\sec^2(\chi_1) + \frac{1}{4} + \frac{\|e_2\|^2}{2}. \tag{25}$$

Furthermore, from Lemma 3, it is easy to show that,

$$\dot{V}_1 \leq -k_1 V_1 + \frac{1}{4} + \frac{\|e_2\|^2}{2}. \tag{26}$$

Now, a positive definitive Lyapunov function is considered as

$$V_2 = \frac{1}{2}e_2^T e_2 + \frac{1}{2}\widetilde{\kappa}^2, \tag{27}$$

where $\widetilde{\kappa} = \kappa - \widehat{\kappa}$ is the estimation error. The time derivative of V_2 can be obtained as

$$\dot{V}_2 = e_2^T \dot{e}_2 - \widetilde{\kappa}\dot{\widehat{\kappa}} = e_2^T(f + gu + d - \dot{\alpha}_1) - \widetilde{\kappa}\dot{\widehat{\kappa}}. \tag{28}$$

By adding and subtracting $\dot{\xi}$, and implementing (14)-(16), (19) and (20) into (28), it is easy to show that

$$\dot{V}_2 = e_2^T(f + d) + N(\xi)\Lambda_2 e_2^T g e_2 - e_2^T\dot{\alpha}_1 - \frac{\widetilde{\kappa}e_2^T e_2\varphi^2}{2} + \sigma\widehat{\kappa}\widetilde{\kappa} + \dot{\xi} - e_2^T\alpha_2. \tag{29}$$

By taking Lemma 2 and (8) into account, one can obtain that

$$e_2^T(f + d) \leq \frac{\kappa e_2^T e_2\varphi^2}{2} + \frac{1}{2}, \tag{30}$$

$$-e_2^T\dot{\alpha}_1 \leq \frac{e_2^T e_2\|\dot{\alpha}_1\|^2}{2} + \frac{1}{2}, \tag{31}$$

$$\sigma\widehat{\kappa}\widetilde{\kappa} \leq \frac{\sigma\kappa^2}{2} - \frac{\sigma\widetilde{\kappa}^2}{2}. \tag{32}$$

On the other hand, as g is square and positive definite, therefore, $g + g^T$ is positive definite. Define, $G_1 = (g + g^T)/2$, $G_2 = (g - g^T)/2$ and

$o_1 = e_2^T G_1 e_2 / e_2^T e_2$, for $\|e_2\| \neq 0$. By using Lemma 5, one can conclude that $\underline{\lambda} \leq \lambda_m(G_1) \leq o_1 \leq \lambda_M(G_1) \leq \overline{\lambda}$, where $\overline{\lambda}$ and $\underline{\lambda}$ are two constants.

Remark 3: As matrix g is unavailable, the parameters o_1, $\underline{\lambda}$, $\overline{\lambda}$, $\lambda_m(G_1)$ and $\lambda_M(G_1)$ are nontrivial to get. However, they are just used for the stability analysis, and not included in the control design. So, their estimation or computation is not required in the proposed design.

Then, it is readily shown that

$$e_2^T G_1 e_2 = o_1 e_2^T e_2. \tag{33}$$

It is worth noting that (33) holds even $\|e_2\| = 0$. This implies o_1 is strictly positive. It is easy to show that $e_2^T g e_2 = e_2^T G_1 e_2 + e_2^T G_2 e_2$. On the other hand, G_2 is a skew-symmetric matrix. Thus, $e_2^T G_2 e_2 = 0$. This further yields that,

$$N(\xi)\Lambda_2 e_2^T g e_2 = o_1 N(\xi)\dot{\xi}. \tag{34}$$

By substituting (30)-(32) and (34) into (29), yields that

$$\dot{V}_2 \leq -c_1 V_2 + c_2 + o_1 N(\xi)\dot{\xi} + \dot{\xi}, \tag{35}$$

where $c_1 = \min\{2k_2, \sigma\}$ and $c_2 = 1 + 0.5\sigma\kappa^2$, which are positive unknown constants. Now to summarize, the following theorem is given.

***Theorem* 1.** Consider the nonlinear robotic manipulator given in (4). Let Assumption 1 hold and the core function $\varphi_0(q, \dot{q})$ be structurally extractable. Let the virtual controllers α_1 and α_2 be designed as in (13) and (15), the control law u be designed as in (14) with the gain (19), and the adaptation laws be constructed as in (16) and (20). Then, (i) All the closed-loop signals are bounded, (ii) The PPB is strictly obeyed by tracking error e_1 right after the given settling time T_s, i.e., $\|e_1(t)\| < \gamma_1$ for $T_s \leq t$ for arbitrary finite initial conditions, and (iii) UUB tracking error is ensured and can be made relatively small by choosing the design parameters properly.

Proof: By multiplying both sides of (35) by $\exp(c_1 t)$ and taking integral over $[0, t]$, one can obtain that

$$V_2(t) \leq \mathfrak{D}_2(t) + e^{-c_1 t}\int_0^t e^{c_1\tau}(o_1 N(\xi(\tau)) + 1)\dot{\xi}(\tau)d\tau, \tag{36}$$

where $\mathfrak{D}_2(t) = (V_2(0) - c_2/c_1)\exp(-c_1 t) + c_2/c_1$. It should be noted that $c_2/c_1 > 0$ and $\lim_{t\to\infty}\exp(-c_1 t) = 0$. Accordingly, $\mathfrak{D}_2(t) \leq \Delta_2$, where $\Delta_2 = c_2/c_1 + V_2(0)$ is an unknown positive constant. Consequently,

$$V_2(t) \leq \Delta_2 + e^{-c_1 t}\int_0^t e^{c_1\tau}(o_1 N(\xi(\tau)) + 1)\dot{\xi}(\tau)d\tau. \tag{37}$$

Furthermore, Δ_2 and c_1 are unknown positive constants. Note that as $o_1 \neq 0$, o_1 satisfies the condition Λ in Lemma 4. Therefore, considering (37) and Lemma 4, it can be shown that V_2 and ξ are bounded over $[0, t]$. Using this, it follows that $\widetilde{\kappa}$, e_2 and $N(\xi(t))$ are bounded. Accordingly, as κ is constant, then $\widehat{\kappa}$ is bounded. Furthermore, it guarantees α_2 and $\dot{\alpha}_1$ are bounded. Therefore, u is bounded. The boundedness of e_2 ensures the existence of constant m such that $\sup_{\tau\in[0,t]}\|e_2(\tau)\| \leq m$. Accordingly, from (26) it is easy to show

$$\dot{V}_1 \leq -k_1 V_1 + c_3, \tag{38}$$

where $c_3 = 0.25 + 0.5m^2$ is an unknown positive constant. By taking integral, (38) furthers yields

$$V_1 \leq \mathfrak{D}_1(t), \tag{39}$$

where $\mathfrak{D}_1(t) = c_3/k_1 + (V_1(0) - c_3/k_1)\exp(-k_1 t)$. It should be noted that $c_3/k_1 > 0$ and $\lim_{t\to\infty}\exp(-k_1 t) = 0$. Accordingly, $\mathfrak{D}_1(t) \leq \Delta_1$, with $\Delta_1 = c_3/k_1 + V_1(0)$ is an unknown positive constant. Consequently, V_1 is bounded as $V_1 \leq \Delta_1$ and hence, z_1 is bounded. On the other hand, as Φ is bounded, shown in Lemma 1, the boundedness of z_1 guarantees e_1 is bounded. Also, as x_d is bounded, then x_1 is bounded. Considering (13), the boundedness of α_1 is ensured. Consequently, x_2 is bounded and thus all signals are bounded.

Considering the scaling function in (9), it is clear that $\|z_1(0)\| = 0$, for arbitrary $e_1(0)$. Accordingly, $z_1(0) \in \Omega_1$, regardless of the initial conditions of e_1. On the other hand, it has been shown that $V_1(t)$ is bounded over $[0, t]$. Thus, by considering the behaviour of the function $\tan(\chi_1)$, one can obtain that $z_1(t) \in \Omega_1$ over $[0, t]$. Also, the inequality $\|\chi_1\| < \pi/2$ is satisfied. This, in turn, leads to $\|z_1(t)\| < \gamma_1$. Note $z_1 = \Phi e_1$ with bounded Φ and $z_1 = e_1$ after the settling time, i.e., $T_s \leq t$. Accordingly, $\|e_1(t)\| < \gamma_1$ for $T_s \leq t$.

Considering (39) and the fact that $\arctan(.)$ is a strictly increasing function, it is readily shown that

$$\|z_1(t)\| \leq \left(\frac{2\gamma_1^2}{\pi}\arctan\left(\frac{\pi}{\gamma_1^2}\mathfrak{D}_1(t)\right)\right)^{0.5}. \tag{40}$$

If $V_1(0) = c_3/k_1$, then $\|z_1(t)\| \leq \left(2\gamma_1^2\arctan(\pi c_3/\gamma_1^2 k_1)/\pi\right)^{0.5} = \Delta^*$, with the design parameter k_1. If $V_1(0) \neq c_3/k_1$, since $\exp(-k_1 t)$ is a decaying function, then there exists T^*, such that $\|z_1(t)\| \leq \Delta^*$ for $t > T^*$, where T^* is an unknown time. On the other hand, as $t\to\infty$, $\|z_1(t)\| \leq \Delta^*$. Therefore, following Definition 2, it is seen that z_1 is UUB. Since $z_1 = e_1$ for $T_s \leq t$ and $\Phi(t)$ is bounded, thus, the tracking error e_1 is also UUB it can be made smaller by choosing design parameters properly. It is worth noting that if $\gamma_1 < \Delta^*$ the time T^* is reached earlier than the preassigned settling time T_s. Otherwise, the tracking error first enters the PPB and then it enters the region $\|z_1(t)\| \leq \Delta^*$. This completes the proof. ■.

Remark 4: The matrix g is positive definite. Then, similar to [41], the term $0.5e_2^T g e_2$ can be used in the Lyapunov function V_2. However, this causes two issues. First, the unknown constant $\bar{g}$, i.e., the largest eigenvalue of g, appears in c_1. Moreover, c_1 adjusts the speed of convergence in (37). Thus, m and, consequently, c_3 will be determined based on $\bar{g}$, which is not a control parameter. In contrast, in this work, only the control parameters adjust the convergence speed. Second, if $0.5e_2^T g e_2$ is used, then the time derivative of M appears in (28). To remove this extra term, it has been usually assumed that the term $\dot{M} - 2H$ is a skew-symmetric matrix [41]. However, this skew-symmetric condition might be violated in some parametrization of the model. For instance, for a non-centroidal body reference frame that is attached to the joint, which is not the center of gravity of the body, this is not satisfied [42]. In this study, this condition is avoided to attribute the general-purpose capacity of the controller.

Remark 5: There are many different BLF functions used in the constrained control framework, see [32] and reference therein. One significant benefit of tangent type BLF (21) in this work is that $\lim_{\gamma_1\to\infty}\gamma_1^2\tan(\chi_1)/\pi = 0.5z_1^T z_1$. This renders the behaviour of quadratic Lyapunov functions for an arbitrarily large bound, despite some other types, e.g. logarithm BLF, or secant BLF. From a practical point of view, this represents a unique characteristic of the proposed controller, which is, whenever it is required to remove the imposed constraints, we can simply choose a large bound, and the designed control is still applicable, with no modification of control structure.

Remark 6: In some similar works, the constraints are imposed on a filtered version of the tracking error [7] or on the tracking error of each joint individually [41]. In both cases, constrained behaviour is achieved. However, in the former one, there is no meaningful interpretation of the imposed constraints. By that means, practically, it is not clear what constraint is imposed on the tracking error itself. On the contrary, this is avoided in the latter one. However, the constraint for each joint leads to a very complicated and numerically expensive approach. In this work, both shortcomings are avoided. As $\|e_1(t)\| < \gamma_1$ is guaranteed for $T_s \leq t$, it can be readily shown that $\|e_{1,i}(t)\| < \gamma_1$ for $T_s \leq t$ and $i = 1, \ldots, n$ and $e_{1,i}$ is the tracking error of i^{th} joint.

Remark 7: Regarding the design parameters, the following points are worth noting. The settling time T_s is determined considering the speed of

the system response. This imposes the time by which the tracking error enters the safety bound from arbitrary initial values. Therefore, if the system response is slow, larger T_s is to be selected to avoid the large control command and, consequent, actuator saturation. Moreover, the parameter ν can impose the desirable speed during the transient period. For faster response, a larger ν is recommended. However, as studied in [43], $\nu = 2$ is recommended. As shown in (35) and (38), k_1 and k_2 impose the exponential convergence to the corresponding sets. Therefore, it is recommended to select large values for these gains to achieve desirable behaviour. On the other hand, parameter σ determines the exponential adaption speed of $\hat{\kappa}$ to a^2. On the other hand, as in (35), σ is to be selected in accordance with k_2, such that the desirable convergence rate of e_2 is achieved, while avoiding the large value of control efforts. Finally, γ_1 is the safety bound on e_1, which is determined by the operational requirements.

3.3. Designed controller features

Here, we highlight some salient features of the designed controller which distinguish it from similar works.

3.3.1. Actuator fault tolerance capability

To discuss the fault tolerance capability in the presence of a variety of actuator faults, modelled by (2), i.e., $\Gamma_1 \neq I_n$ and $\Gamma_2 \neq 0_{n\times 1}$, the following Theorem is given.

Theorem 2. Consider the nonlinear robotic manipulator given in (4). Let Assumption 1 hold and the core function $\varphi_0(q,\dot{q})$ be structurally extractable. Let the virtual controllers α_1 and α_2 be designed as in (13) and (15), the control law u be designed as in (14) with the gain (19), and the adaptation laws be constructed as in (16) and (20). In the presence of the actuator effectiveness loss $\Gamma_1 \neq I_n$ and bias $\Gamma_2 \neq 0_{n\times 1}$, the objectives (i)-(iii), presented in Theorem 1, are satisfied.

Proof. In the faulty case, the derivation of (21)-(26) is still valid. The bias Γ_2 has been already encapsulated in d and the inequality (8) is still applicable. Thus, the effectiveness loss Γ_1 is taken into account. The time derivative of V_2 is obtained as

$$\dot{V}_2 = e_2^T\dot{e}_2 - \tilde{\kappa}\dot{\hat{\kappa}} = e_2^T(f + g\Gamma_1 u + d - \dot{\alpha}_1) - \tilde{\kappa}\dot{\hat{\kappa}}. \tag{41}$$

Considering g and Γ_1 are both positive definite matrices, then $\mathscr{G} = g\Gamma_1$ is a square positive definite matrix. Thus, $e_2^T g\Gamma_1 u = N(\xi)\Lambda_2 e_2^T\mathscr{G}e_2$. Note that $\mathscr{G}+\mathscr{G}^T$ is positive definite. Define, $\mathscr{G}_1 = (\mathscr{G} + \mathscr{G}^T)/2$, $\mathscr{G}_2 = (\mathscr{G} - \mathscr{G}^T)/2$ and $o_2 = e_2^T\mathscr{G}_1 e_2/e_2^T e_2$, for $\|e_2\| \neq 0$. By using Lemma 5, one can conclude that $\underline{\lambda}^* \leq \lambda_m(\mathscr{G}_1) \leq o_2 \leq \lambda_M(\mathscr{G}_1) \leq \overline{\lambda}^*$, where $\underline{\lambda}^*$ and $\overline{\lambda}^*$ are two constants. Then, it is readily shown that

$$e_2^T\mathscr{G}_1 e_2 = o_2 e_2^T e_2. \tag{42}$$

It is worth noting that (42) holds even $\|e_2\| = 0$. This implies o_2 is strictly positive. It is easy to show that $e_2^T\mathscr{G}e_2 = e_2^T\mathscr{G}_1 e_2 + e_2^T\mathscr{G}_2 e_2$. On the other hand, $\mathscr{G}_2$ is a skew-symmetric matrix. Thus, $e_2^T\mathscr{G}_2 e_2 = 0$. Therefore, it can be obtained that

$$V_2(t) \leq \Delta_2 + e^{-c_1 t}\int_0^t e^{c_1\tau}(o_2 N(\xi(\tau)) + 1)\dot{\xi}(\tau)d\tau. \tag{43}$$

Note that as $o_2 \neq 0$, o_2 satisfies the condition Λ in Lemma 4. The rest of this proof is similar to that of Theorem 1 (see from (37) to the end of proof) and thus omitted. ■.

3.3.2. Handling actuator backlash hysteresis

The i^{th} actuator of the robotic manipulator may suffer from hysteresis in long term operation. This causes a cyclic difference between commanded control on i^{th} actuator, u_i, and the actual actuator effort $u_{a,i}$. Based on Duhem backlash-like model [1], the actuator hysteresis can be modelled as

$$\frac{d(u_{a,i}(u_i))}{dt} = \gamma_{h,i}\left|\frac{du_i}{dt}\right|(\delta_{h,i}u_i - u_{a,i}(u_i)) + \beta_{h,i}\frac{du_i}{dt}, \tag{44}$$

for $i = 1,\ldots,n$, where $\gamma_{h,i}$, $\delta_{h,i}$ and $\beta_{h,i}$ are unknown positive constants. $\delta_{h,i}$ is the slope of the hysteresis line and $\delta_{h,i} > \beta_{h,i}$. This can be written as

$$u_{a,i}(u_i) = \delta_{h,i}u_i + \epsilon_{h,i}(u_i), \tag{45}$$

with, $\epsilon_{h,i}(u_i) = (u_{a,i}(u_i(0)) - \delta_{h,i}u_i(0))e^{-\gamma_{h,i}(u_i(t)-u_i(0))sign(\dot{u}_i)} + e^{-\gamma_{h,i}u_i(t)sign(\dot{u}_i)}\int_{u_i(0)}^{u_i(t)}(\beta_{h,i} - \delta_{h,i})e^{-\gamma_{h,i}sign(\dot{u}_i)\tau}d\tau$. Accordingly, $\epsilon_{h,i}(u_i)$ is bounded as $|\epsilon_{h,i}(u_i)| \leq \overline{\epsilon}_{h,i}$, where $\overline{\epsilon}_{h,i}$ is an unknown positive constant [1]. Now considering i^{th} row of (2), one can obtain that $u_{a,i} = \gamma_{i,1}\left(t - t_{f_{i,1}}\right)u_i + \gamma_{i,2}\left(t, t_{f_{i,2}}\right)$. Therefore, one significant characteristic of the presented fault model (2), is that it can be adjusted to present the hysteresis phenomenon. In this case, we choose $t_{f_{i,1}} = t_{f_{i,2}}$ the moment at which the hysteresis happens. On the other hand, for the given $\delta_{h,i}$, it can be modelled by $\gamma_{i,1}$ and a_i and b_i are adjusted. That is, the bounded additive bias $\gamma_{i,2}$ is replaced by $\epsilon_{h,i}(u_i)$. Therefore, in accordance with Theorem 2, we can conclude that the objectives (i)-(iii), presented in Theorem 1, are satisfied, even in the presence of hysteresis. For brevity, the proof of Theorem 2 is not repeated here.

3.3.3. Handling uncertain initial conditions

In most of the existing works [32,33,35] the initial condition $e_1(0)$ is considered known, and assumed to lie within the given constraint, i.e., $\|e_1(0)\| < \gamma_1$. However, the proposed method in this work can handle different initial conditions and the settling time T_s can be selected as a small value. When the initial condition is known but outside of the PPB, i.e., $\|e_1(0)\| > \gamma_1$, most of the available works are inapplicable. In this case, the boundedness of $\gamma_1^2\tan(0.5\pi e_1^T e_1/\gamma_1^2)/\pi$ does not imply $\|e_1(t)\| < \gamma_1$, taking into account two vertical asymptotes of $\tan(0.5\pi e_1^T e_1/\gamma_1^2)$ at $\|e_1(t)\| = \pm\gamma_1$. One trivial solution is to enlarge the PPB according to the given initial condition. This is investigated in some works with exaggeratedly large PPB e.g. [33], or with a decaying time variable constraint e.g. [32]. The former one is useless in practice considering a small safety bound as the PPB. While the latter one imposes the complicated algorithms including the time derivative of the constraint. This further increases the real-time computational cost. In contrast, our approach can address the issues mentioned while no controller modification is required, by incorporating the scaling function.

In the case of unknown/uncertain initial conditions, i.e., $e_1(0)$ is unavailable, the regular BLF-based methods [33,35] fail to operate satisfactorily, or even unstable, as the initial condition might be outside of the PPB and there is no information to shape the constraints. Indeed, if it is not ensured that the initial tracking error is within the PPB, then the boundedness of BLF does not mean the tracking error stays in PPB. In contrast, in our approach, for even uncertain initial conditions, it is guaranteed that $\|z_1(0)\| = 0$ and hence, $z_1(0) \in \Omega_1$.

Finally, if the constraint is imposed on a system sometime after the system starts to operate, then the available designs are not guaranteed to fulfil the PPB specification. In this case, the regular BLF-based methods in [32,33,35] require the assumption $\|e_1(t_0)\| \leq \gamma_1$, where t_0 is the moment the constraint is imposed. However, our proposed method desirably works no matter the constraint is imposed when the system operation starts, or in the middle of the operation.

4. Simulation results and discussion

In this section, the performance of the proposed approach is evaluated using the PUMA560 robotic benchmark model, with a dynamics model and parameters given in [44]. It is worth noting that this benchmark model is widely adopted in similar works to verify the

control performance. The performance of the proposed controller is evaluated through several scenarios including actuator fault, backlash and hysteresis, variable initial conditions, and variable control gains. The friction and disturbance terms are modelled as [4].

$$F(\dot{q})+\tau_d=\begin{bmatrix}0.5\dot{q}_1+\sin(3q_1)+0.5\sin(\dot{q}_1)\\ 1.3\dot{q}_2-1.8\sin(2q_2)+1.1\sin(\dot{q}_2)\\ -1.8\dot{q}_3+2\sin(3q_3)+0.15\sin(\dot{q}_3)\end{bmatrix}.$$

Also, the desired trajectory is selected as $x_d(t)=\left[\cos(t/5\pi)-1,\cos\left(\frac{t}{5\pi}\right)-1,\sin\left(\frac{t}{5\pi}+\frac{\pi}{2}\right)-1\right]^T$ [45]. The proposed controller parameters are selected as $k_1=200$, $k_2=300$, $\gamma_1=0.1(rad)$, $\sigma=1$, $T_s=5(s)$, $\nu=2$, with the core function $\varphi_0(q,\dot{q})=\|\dot{q}\|^2+\|\dot{q}\|+1$. Moreover, the state-of-the-art controllers are adopted to compare the results, to highlight the corresponding drawbacks which are resolved by the proposed method. The adopted controllers are PID [46], sliding mode PID (SMPID) [47], Logarithm type BLF (LogBLF) [48] and Tangent type BLF (TanBLF) [34].

We have considered two different initial conditions, i.e., $Set1=[0,0,0]^T$ and $Set2=[0,-\pi/3,-\pi/10]^T$. Considering $Set1$, $\|e_1(0)\|=0$ and, hence, it lies within the PPB with $\gamma_1=0.1(rad)$. On the other hand, for $Set2$, $\|e_1(0)\|=1.093$ which is greater than γ_1. Therefore, it is initially out of the given bound. $Set2$ is used to study the importance of the incorporated scaling function. For the sake of comparison, the root mean squared of tracking error is used as a numerical metric, defined as $E_i=\sqrt{\sum_{k=1}^{N}e_{1,i}^2(k)/N}$, where N is the sampling time number, $i=1,2,3$ denotes the joint number, and $e_{1,i}(k)$ is the tracking error of i^{th} joint at k^{th} sample time.

4.1. Scenario 1: tracking performance in normal condition

Initially, we assume that the system is operated in fault-free condition with the initial condition $Set1$. The tracking performance is illustrated in Figs. 1 and 2. It can be seen that the proposed controller is able to track the desired trajectory with the tracking error within the PPB. Also, the transient response has been smoothly passed and the states have converged to the desired ones. The PID control is not able to satisfy the mentioned characteristics. Furthermore, considering the tracking of joint 2, the transient time of SMPID and LogBLF is longer than TanBLF control. Therefore, this motivates the choice of tangent type BLF in our proposed control. These are confirmed via numerical comparison given in Table 2, indicating the more accurate tracking performance of the proposed controller compared to the PID and LogBLF ones. The control effort is shown in Fig. 3. The estimated parameter $\widehat{\kappa}$ is depicted in Fig. 4. Evidently, the estimated signal and the control signal are smooth and bounded.

Table 2
Numerical comparison of the proposed controller performance with the benchmark controllers for Scenarios 1–5. PC denotes proposed controller.

	Operating Conditions					
	Scenario 1			Scenario 2		
	E_1	E_2	E_3	E_1	E_2	E_3
PID	$5.1e^{-4}$	0.0341	0.0142	$6.77e^{+3}$	$2.25e^{+4}$	400
SMPID	$9.9e^{-6}$	$8.01e^{-4}$	$5.07e^{-5}$	$5.1e^{-4}$	$1.43e^{3}$	6.783
LogBLF	$2.6e^{-5}$	0.001	$1.3e^{-4}$	0.057	0.073	0.011
TanBLF	$1.75e^{-8}$	$1.75e^{-8}$	$1.75e^{-8}$	$6.29e^{-4}$	$3.63e^{-4}$	$1.75e^{-8}$
PC	$3.58e^{-4}$	$3.73e^{-4}$	$3.77e^{-4}$	$3.87e^{-4}$	$4.96e^{-4}$	$1.3e^{-4}$
	Scenario 3			Scenario 4		
	E_1	E_2	E_3	E_1	E_2	E_3
PID	0.001	0.014	0.0058	0.01	0.126	0.03
SMPID	$7.32e^{-4}$	0.002	$7.34e^{-4}$	0.2057	27.38	1.07
LogBLF	0.0013	0.065	0.0405	0.002	0.095	0.04
TanBLF	$4.02e^{-6}$	$4.82e^{-5}$	$1.39e^{-4}$	$9.31e^{-7}$	0.147	0.04
PC	$3.58e^{-4}$	$3.73e^{-4}$	$3.74e^{-4}$	0.001	0.061	0.02
	Scenario 5					
	E_1	E_2	E_3			
PID	$5.1e^{-4}$	0.0341	0.0142			
SMPID	$9.9e^{-6}$	$8.01e^{-4}$	$5.07e^{-5}$			
LogBLF	$2.6e^{-5}$	0.001	$1.3e^{-4}$			
TanBLF	$1.75e^{-8}$	$1.75e^{-8}$	$1.75e^{-8}$			
PC	$3.58e^{-4}$	$3.73e^{-4}$	$3.77e^{-4}$			

4.2. Scenario 2: fault tolerance capability

To evaluate the fault-tolerant features of the proposed controller, the fault is modelled using (2) and (3) with parameters $t_{f_{1,1}}=0$, $b_1=0$, $a_1=0$, $t_{f_{2,1}}=30$, $b_2=0.15$, $a_2=10$, $t_{f_{3,1}}=0$, $b_3=0$, $a_3=0$, $\gamma_{1,2}(t,20)=30\sin(q_1q_2)+4\cos(\dot{q}_1q_2)+15\cos(\dot{q}_1q_2)$ and $\gamma_{2,2}(t,0)=\gamma_{3,2}(t,0)=0$. This fault model imposes an additive fault $\gamma_{1,2}(t,20)$ on the first joint actuator after 20 (s). Also, as a_2 is large, an abrupt effectiveness loss of 15% is applied on the second joint actuator after 30 (s). It should be noted that the proposed FTC design belongs to the passive FTC category, where distinguishing between faults and disturbances, as well as identifying the fault time and amplitude, are not concerns for the controller. This aspect can be effectively addressed by the FDI system [49,50], which is beyond the scope of this study.

The tracking performance and control signal are shown in Figs. 5 and 6, respectively. Also, the estimated $\widehat{k}$ is depicted in Fig. 7. It is obvious that PID and SMPID controllers become unstable with a very large control signal. To accurately investigate the results, the tracking performance of TanBLF, LogBLF and proposed controllers are separately illustrated in Figs. 8–10. Additionally, considering the results of Table 2, it is obvious that tracking error is retained within the PPB with a short transient response. Again, the tracking error using the proposed controller is smaller than LogBLF.

It is worth mentioning that, by investigating several numerical simulations, other controllers fail to perform satisfactorily for the actuator effectiveness loss of more than 15%. In contrast, the proposed controller is still able to meet the PPB with the given transient time. To investigate this, as suggested in [4], the effectiveness loss of 80% is applied on the actuator of the joint 2, i.e., $b_2=0.8$. The results are given in Figs. 11 and 12. These figures highlight the salient feature of the fault-tolerant performance of the proposed controller and confirm its superiority against the other counterparts. This feature stems from the incorporation of the Nussbaum type function into the control structure, see (14) and (19).

4.3. Scenario 3: actuator backlash/ hysteresis

To study the effect of the cyclic difference between commanded control on i^{th} actuator, u_i, and the actual actuator effort $u_{a,i}$, Duhem backlash- hysteresis model (44) is used with parameters are set as $\gamma_{h,i}=1$, $\delta_{h,i}=1.16$ and $\beta_{h,i}=0.35$ on all the actuators, which are unknown constants. The tracking performance is illustrated in Fig. 13. The control signal is depicted in Fig. 14. The superior performance of the proposed controller is obvious here, as it is numerically confirmed in Table 2. It can be seen that the performance of PID and LogBLF controllers are degraded due to the effect of backlash- hysteresis. Moreover, considering Table 2, the joint 2 tracking error is large using SMPID, compared to the proposed controller. The cyclic variation of the actuator effort leads to the tracking error variation off the sliding surface. Finally, the PPB is satisfied using the proposed controller.

4.4. Scenario 4: initial conditions out of the PPB

To study the performance in this case, which is one of the main characteristics of the proposed method, the initial conditions are selected as $Set2$, which are outside of the PPB. As shown in Fig. 15, the preassigned settling time $T_s=5$secis achieved. Also, the tracking error is retained in PPB after T_s, as shown in Fig. 16. The control signal is

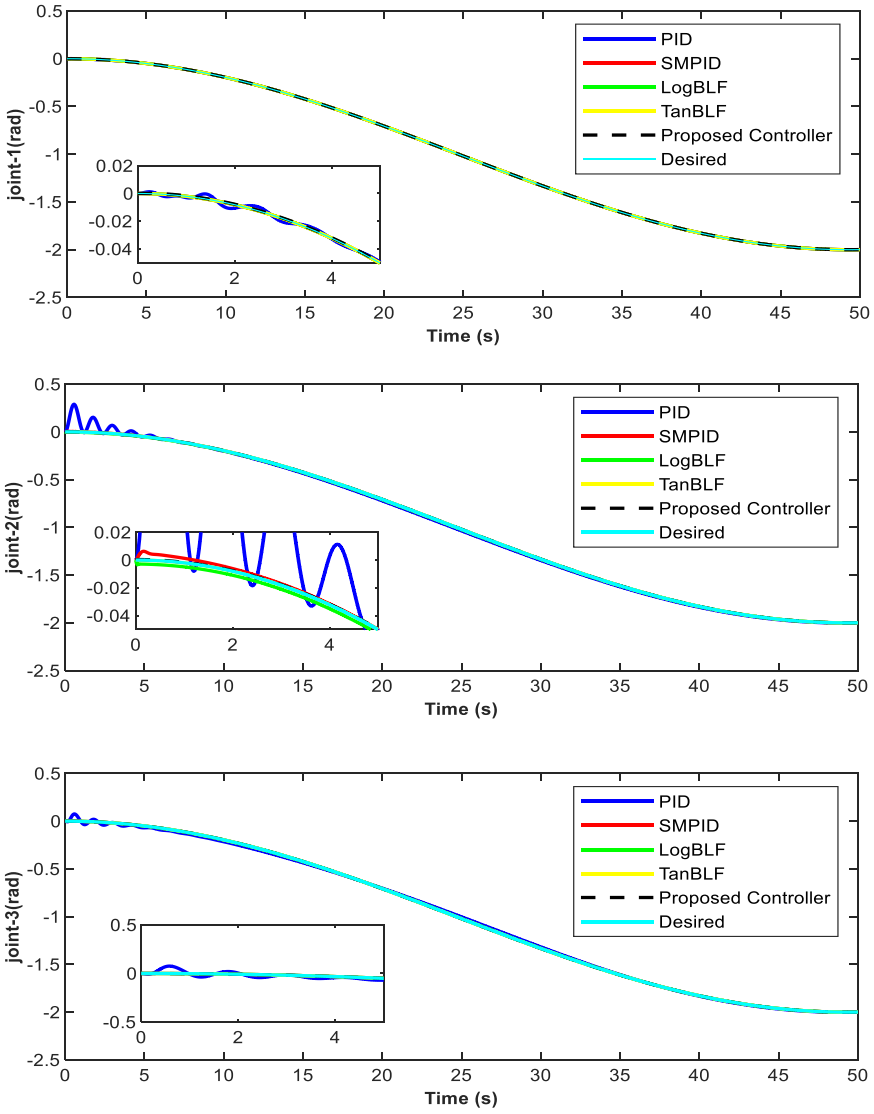

Fig. 1. Tracking performance in normal condition.

presented in Fig. 17. The performance of other controllers with initial conditions out of the PPB is depicted in Figs. 18 and 19 as well as the control signals are shown in Fig. 20. It is seen that the control signals for TanBLF and LogBLF present overshoot. However, this overshoot is not encountered using the proposed controller. This represents one of the key features of this work over the considered controllers. This stems from the initial conditions out of PPB. Considering the tracking performance as well as the magnitude of the control signal, it can be concluded that the proposed controller outperforms the other benchmark controllers, thanks to the use of the scaling function of (9). This dominant performance is numerically confirmed in Table 2.

4.5. Scenario 5: uncertain inertia matrix

As given in (4), the control gain is $g(q) = M^{-1}(q)$. Therefore, in the case of uncertainty in the inertia matrix, the control gain changes, and accordingly, it is unknown. To implement this scenario, the uncertainty is added to the original inertia matrix at $T = 10$sec. This uncertainty is implemented as a matrix with random numbers. The random process is modelled as a stochastic process with Gaussian distribution and the mean value of the corresponding nominal values.

The tracking performance, error, and control signal are shown in Figs. 21–23, respectively. As inferred from the performance evaluation, the proposed controller can compensate for the effect of model uncertainty. This is numerically verified in Table 2. This performance is due to the incorporation of $N(\xi)$ in (14) that resolves the unknown gain problem. While in the other controllers nominal $M(q)$ is used in the structures.

5. Conclusion

This paper presents a control method for a robotic manipulator enhancing the prescribed trajectory tracking performance for a wide range of operating conditions. The proposed control system used the adaptive backstepping approach combined with a tangent-type barrier Lyapunov function to preserve fast response and user-defined settling time while ensuring the stability of the manipulator even under actuation fault or backlash/hysteresis phenomena. The salient features of the proposed method guarantee a PPB and relax the assumption of the bounded initial condition by incorporating a well-defined scaling function that maintains the safety bound for the manipulator working in hazardous and cluttered environments for real-time application. The proposed method is applied to the PUMA560 robotic manipulator model, and its performance is investigated via extensive simulation studies and against several benchmark controllers. The simulation results confirmed the superior performance of the proposed controller

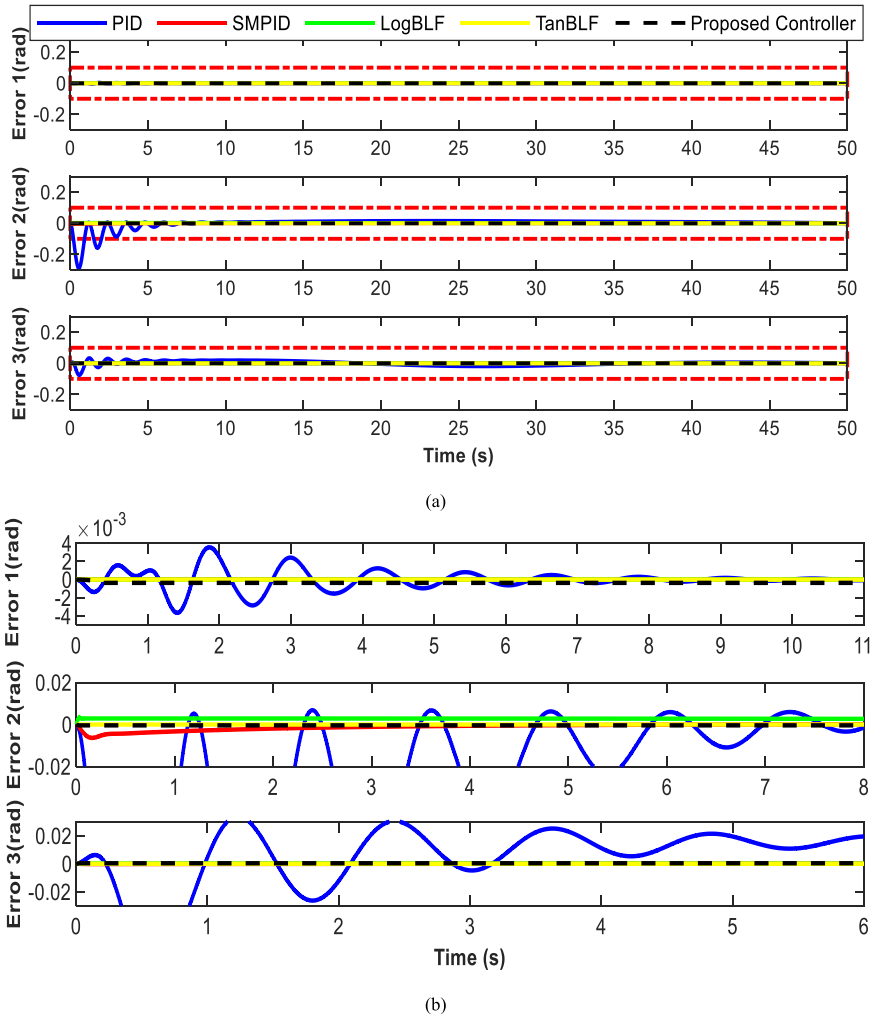

Fig. 2. Tracking errors in normal condition (Dashed red lines denote the PPB) (a); zoom-in view (b).

against the benchmark counterparts in efficiently and robustly handling operating conditions such as actuator fault and backlash/ hysteresis, initial conditions out of the PPB, and variable control gain due to model uncertainty. The future direction of this study is field trials and experimental validation of the proposed control method.

Declaration of Competing Interest

Authors declare that there is no conflict of interest with this submission.

Appendix

To assess the performance of the proposed controller against a fast reference trajectory, the frequency of the desired trajectory $x_d(t)$, as discussed in Section IV, is increased by 5π. In other words, the new desired trajectory is given by:

$$x_{d\_new}(t) = \left[\cos(t) - 1, \cos(t) - 1, \sin\left(t + \frac{\pi}{2}\right) - 1\right]^T$$

Subsequently, the trajectory tracking performance is evaluated under two conditions: normal operating condition (Scenario 1) and actuator fault (Scenario 2). It should be noted that apart from the change in the desired trajectory, all other conditions and settings used in Scenarios 1 and 2 remain unchanged.

Figures A-1- A-6 demonstrate the tracking performance of the proposed controller in normal and under fault conditions. As can be inferred from the figures, the proposed controller enables fast tracking of the new desired trajectory while maintaining the control performance criteria, specifically in terms of tracking error within the PPB and control signal, as provided in Scenarios 1 and 2 previously.

It should be noted that in practice, employing a sinusoidal reference signal with a frequency of 5π (approximately 15.7 Hz), which is close to or even exceeds the natural resonant frequency of the PUMA 560 system [51], can give rise to some challenges and potential issues in tracking performance, such as the occurrence of resonance effects. These effects can magnify vibrations and oscillations within the system, rendering it challenging to maintain control and potentially resulting in instability. Furthermore, this approach may result in unexpected behavior, elevated mechanical stresses, and the risk of damaging the robot.

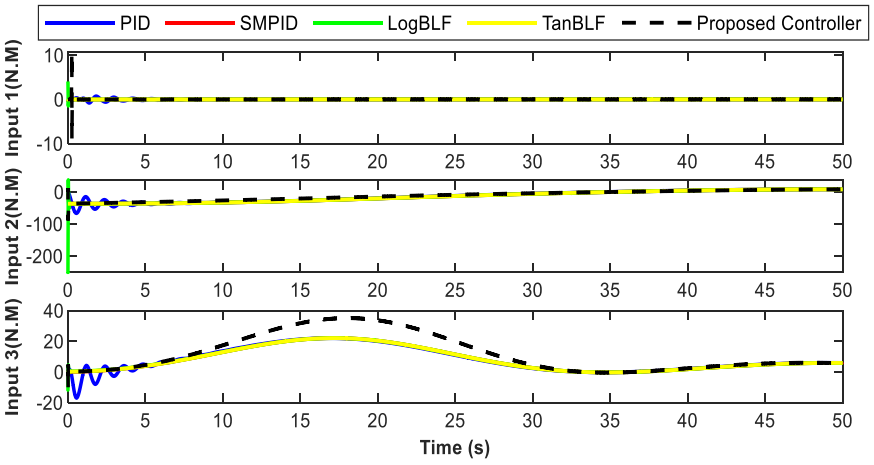

(a)

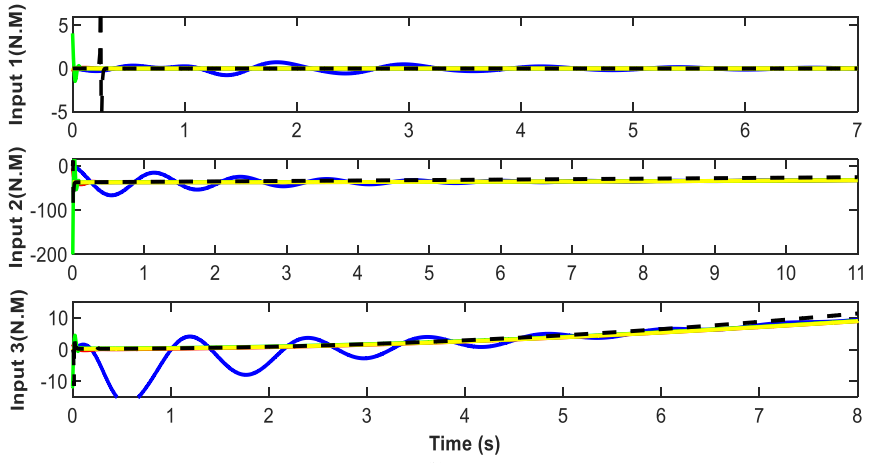

(b)

Fig. 3. The control signal in normal condition.; zoom-in view (b).

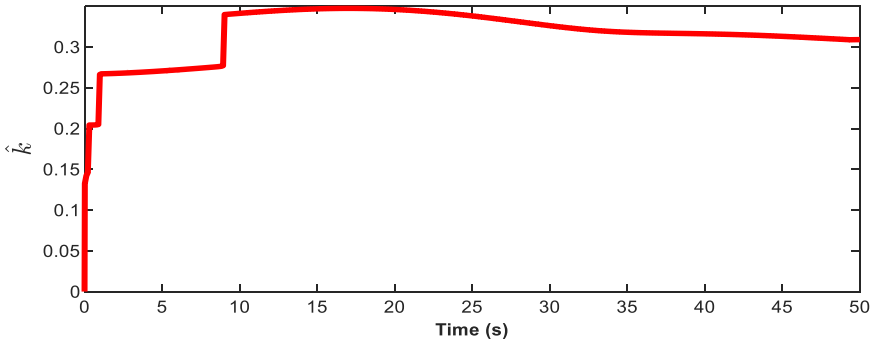

Fig. 4. Estimated $\widehat{k}$ in normal condition.

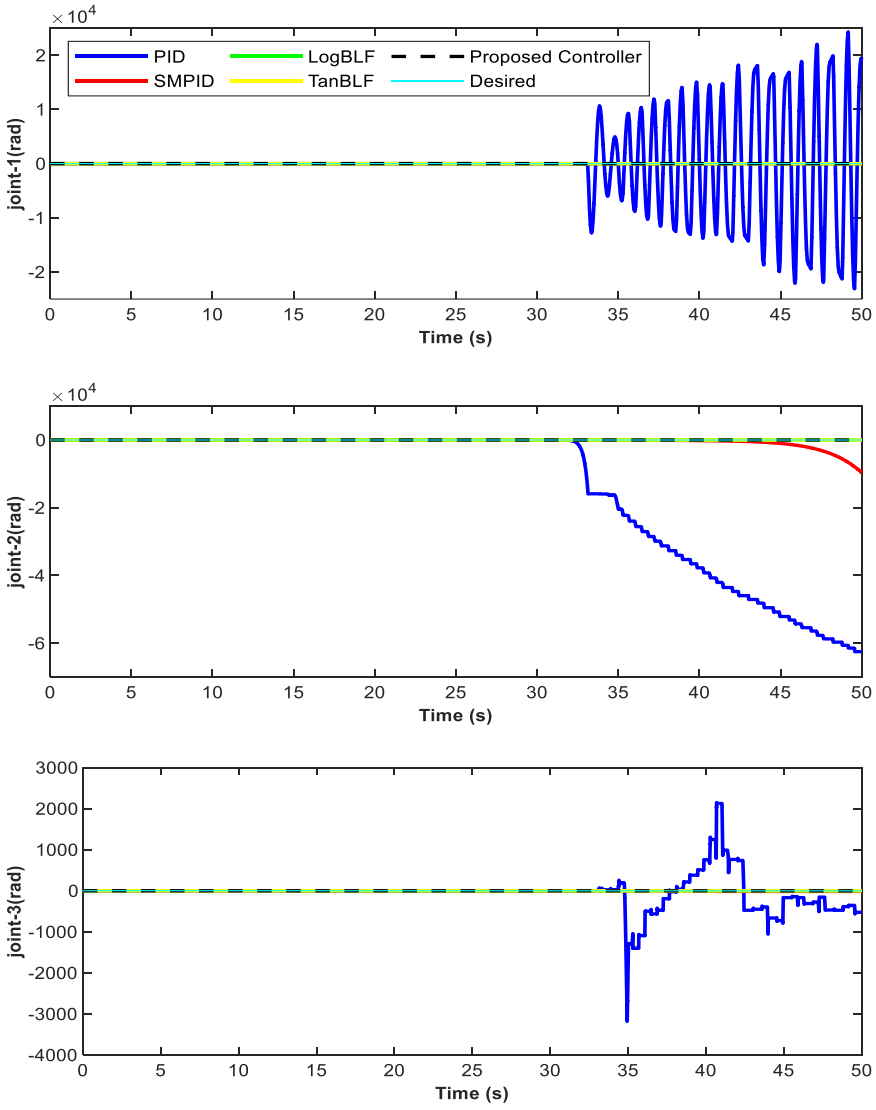

Fig. 5. Tracking performance under actuator fault.

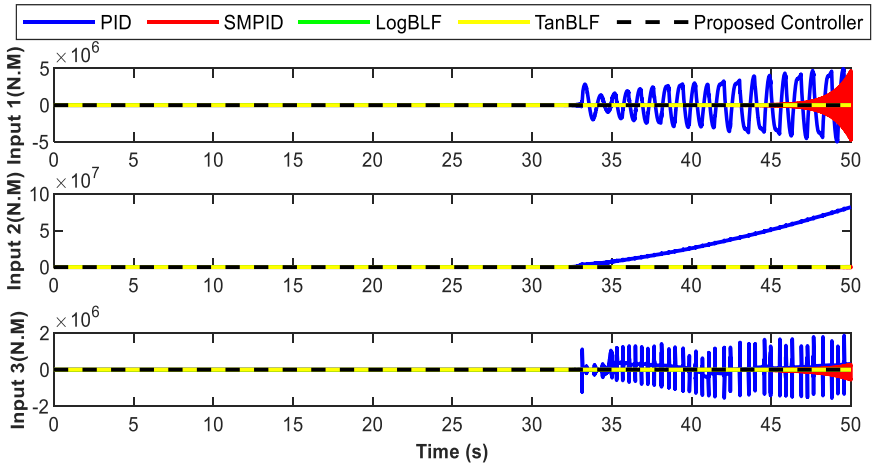

Fig. 6. The control signal under actuator fault.

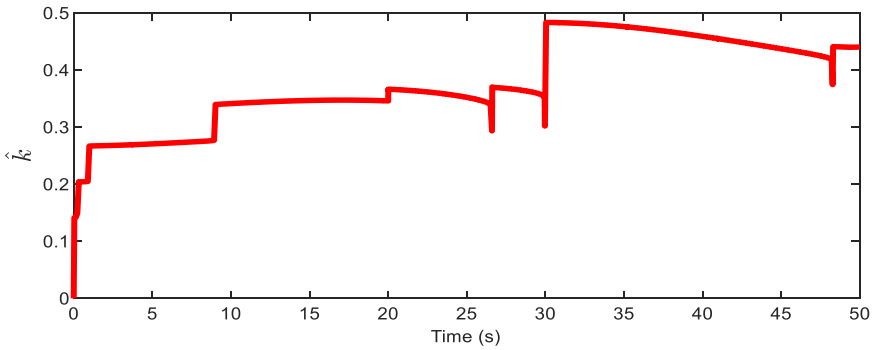

Fig. 7. Estimated $\widehat{k}$ under actuator fault.

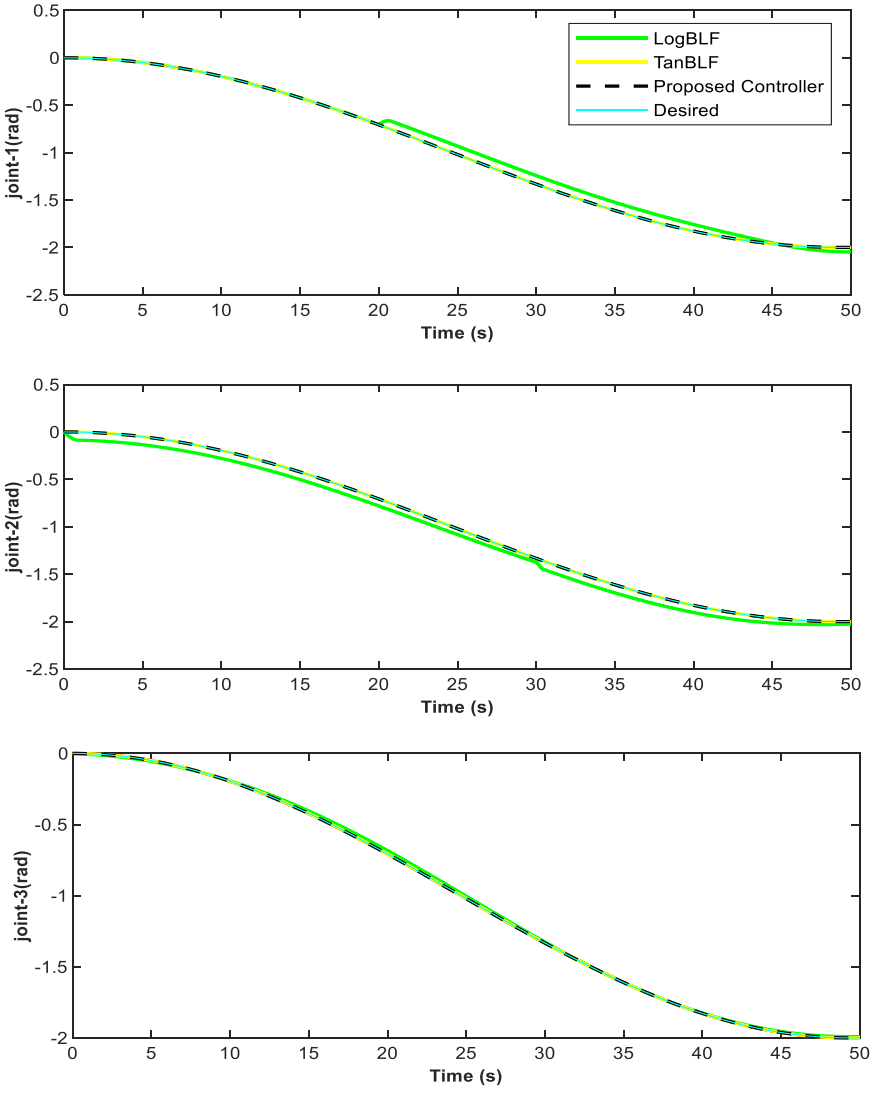

Fig. 8. Tracking performance of TanBLF, LogBLF and proposed controllers under actuator fault.

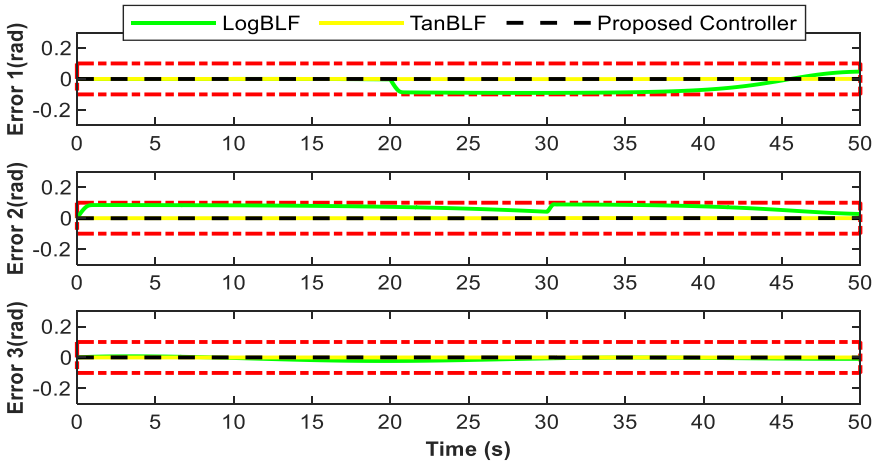

Fig. 9. Tracking error of TanBLF, LogBLF and proposed controllers under actuator fault (Dashed red lines denote the PPB).

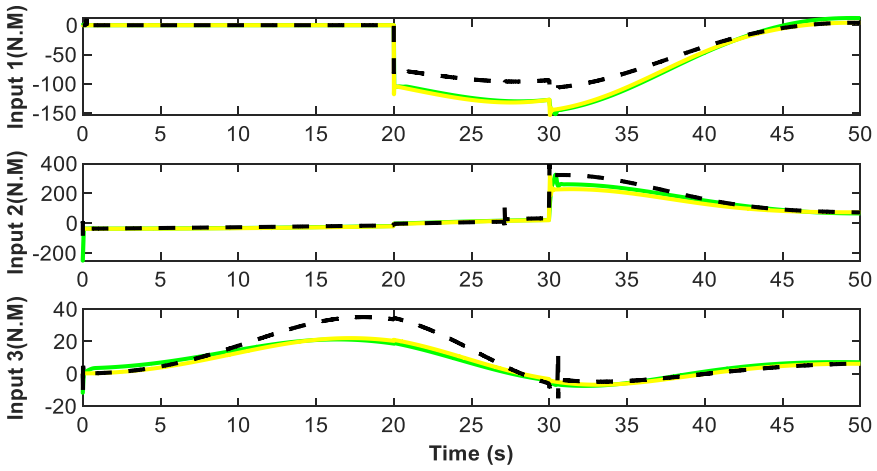

Fig. 10. The control signal of TanBLF, LogBLF and proposed controllers under actuator fault.

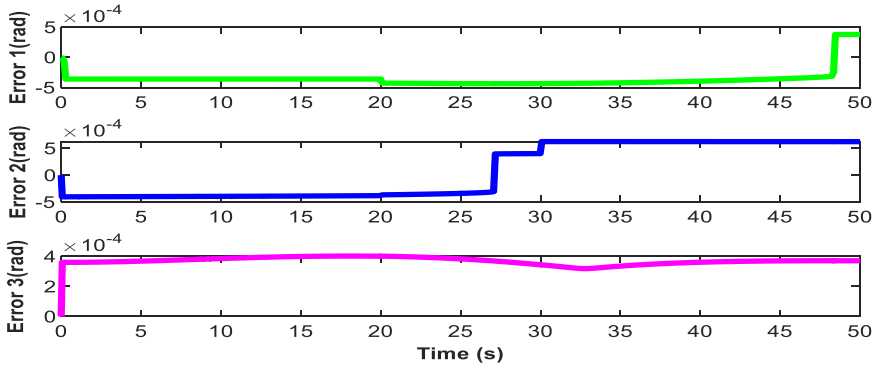

Fig. 11. Tracking error of proposed controllers under fault $b_2 = 0.8$.

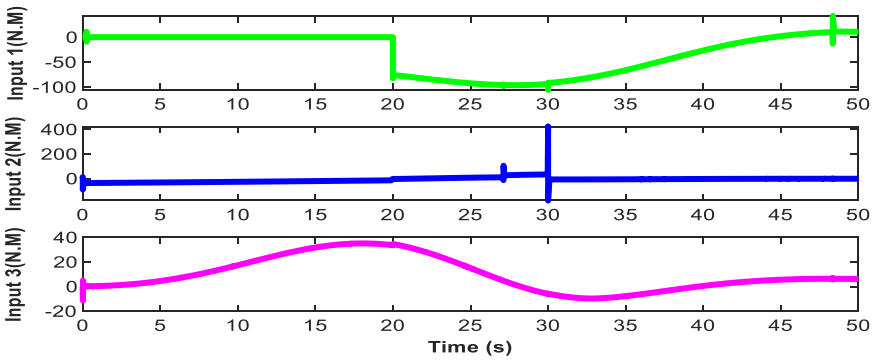

Fig. 12. The control signal of the proposed controller under fault $b_2 = 0.8$.

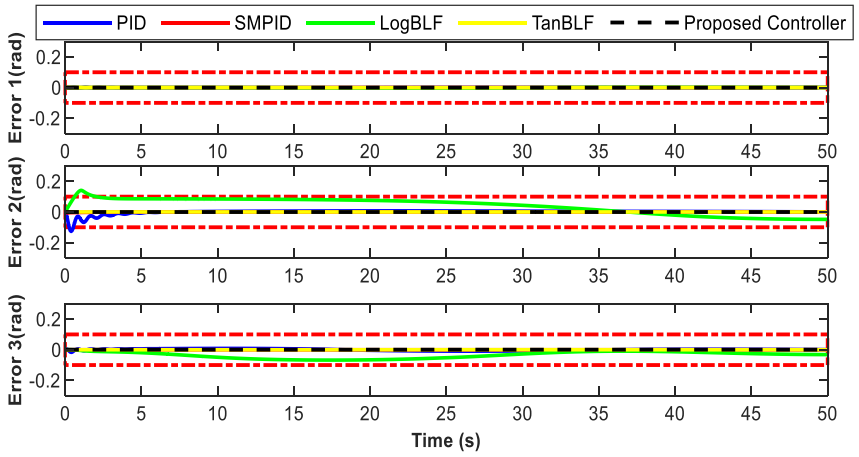

(a)

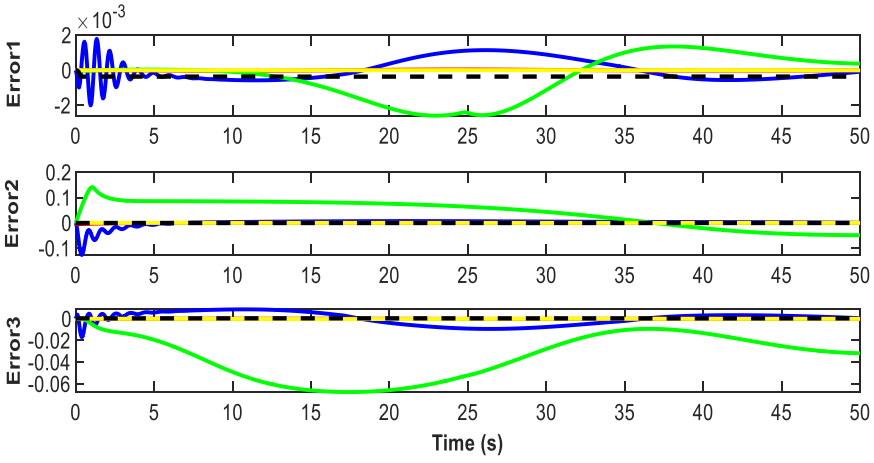

(b)

Fig. 13. Tracking error under actuator backlash (Dashed red lines denote the PPB) (a); zoom-in view (b).

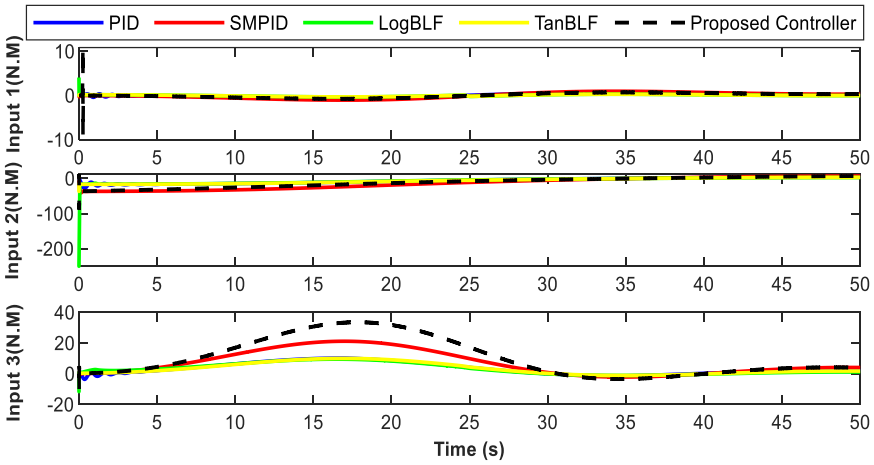

Fig. 14. The control signal in Backlash/ Hysteresis condition.

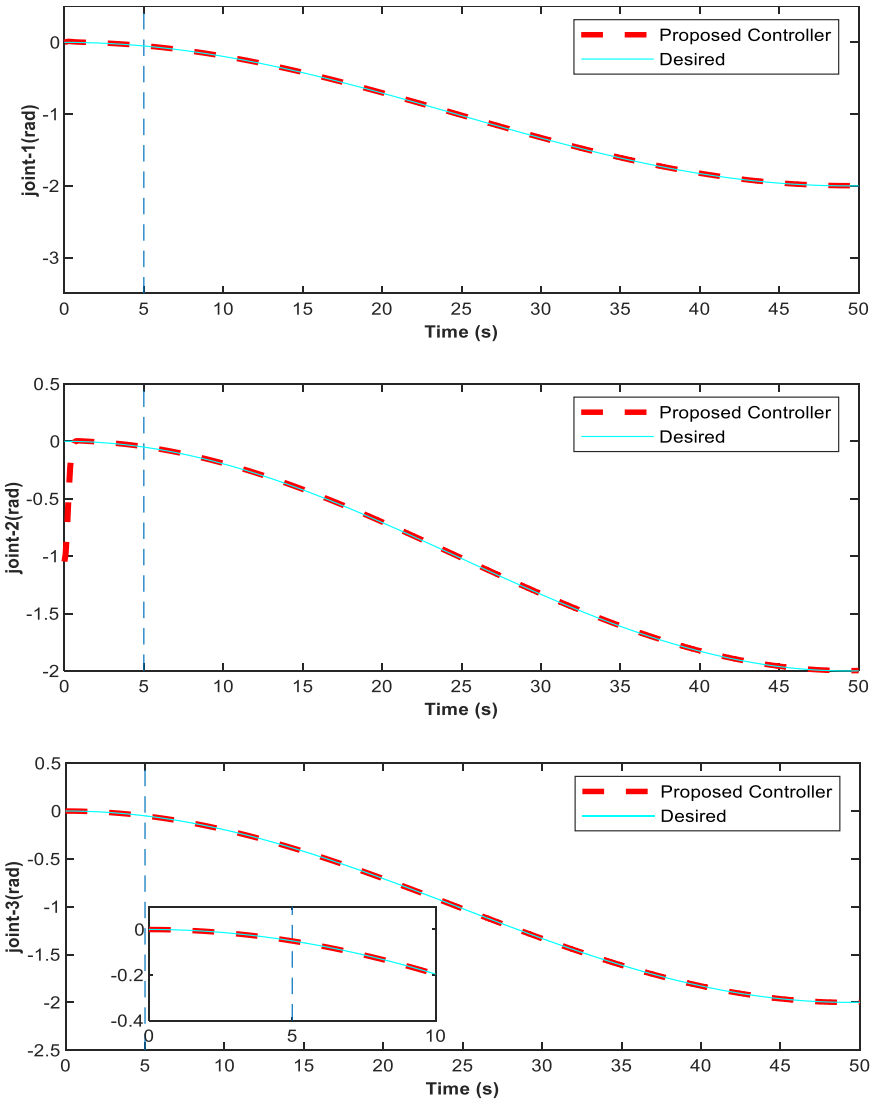

Fig. 15. Tracking performance of the proposed controller with initial conditions out of the PPB.

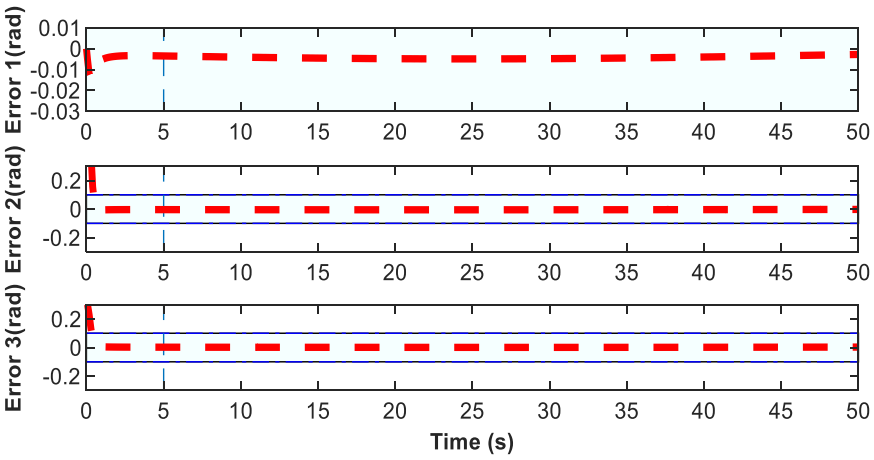

Fig. 16. Tracking error of the proposed controller with initial conditions out of PPB.

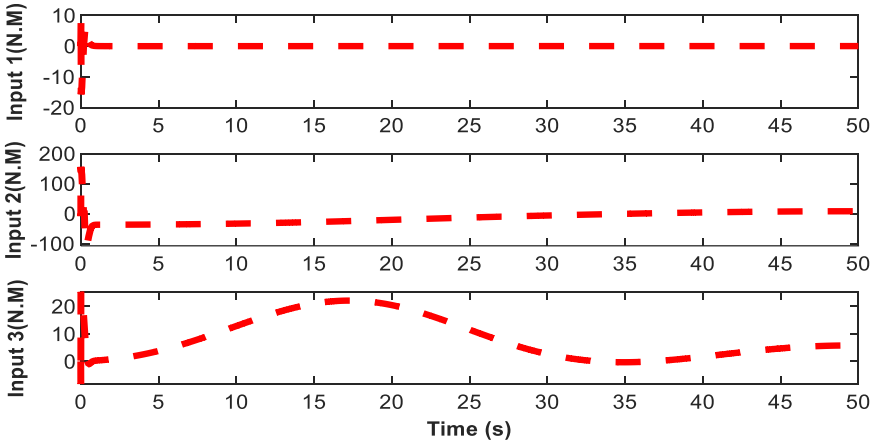

Fig. 17. The control signal of the proposed controller with initial conditions out of the PPB.

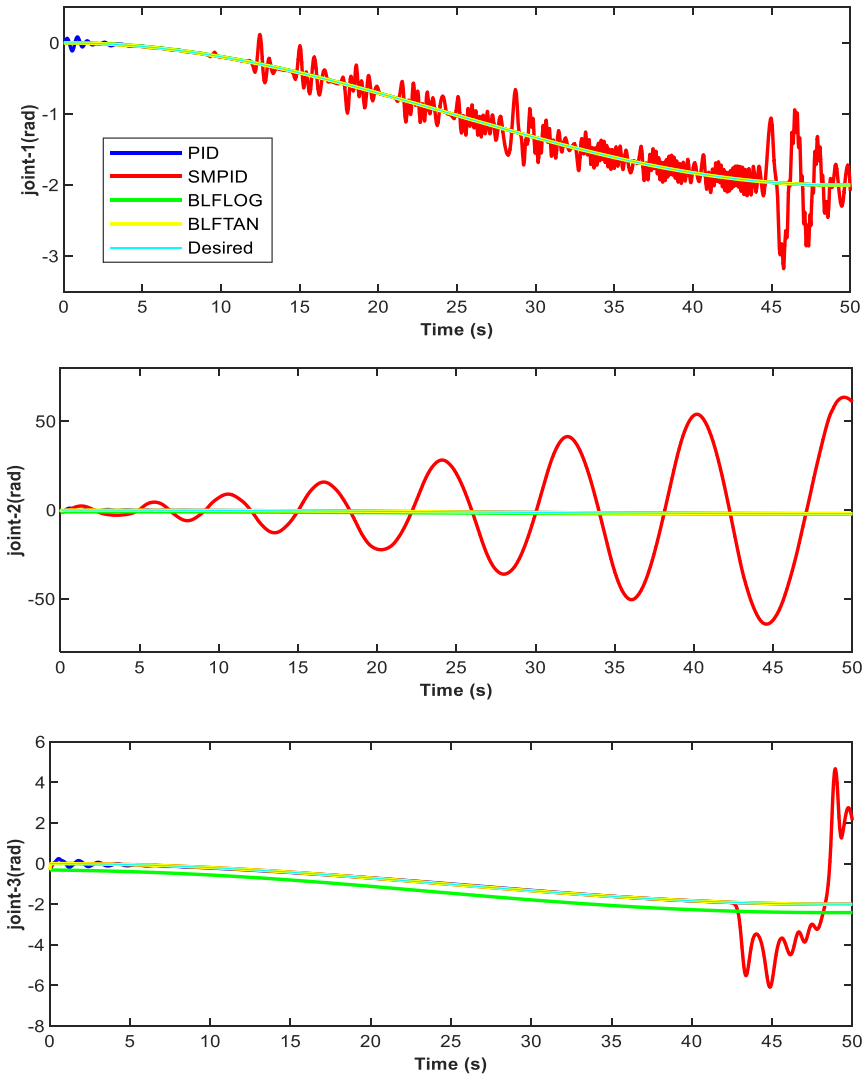

Fig. 18. Tracking performance with initial conditions out of the PPB.

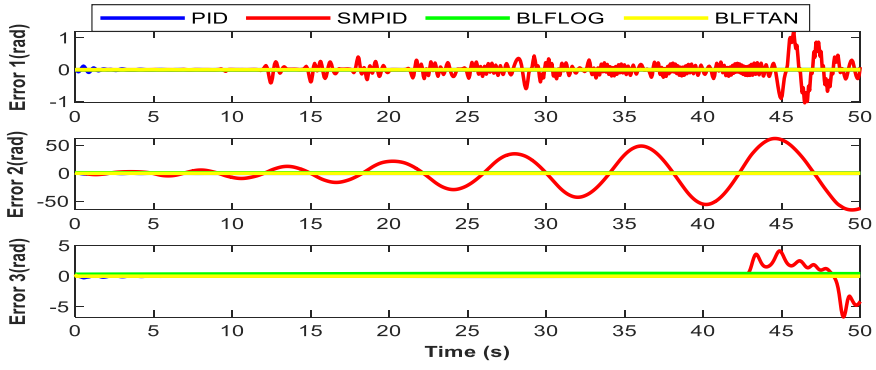

Fig. 19. Tracking error for Initial conditions out of the PPB.

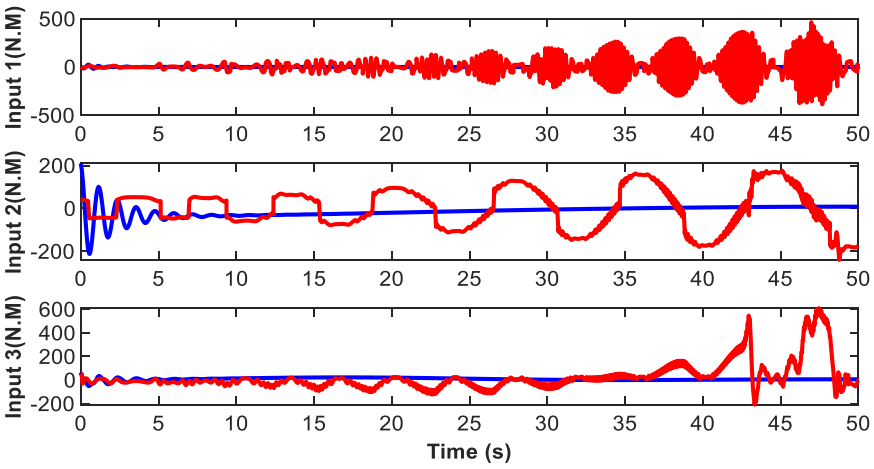

Fig. 20. The control signal for initial conditions out of the PPB for benchmark controllers (a); zoom-in view for PID and SMPID (b).

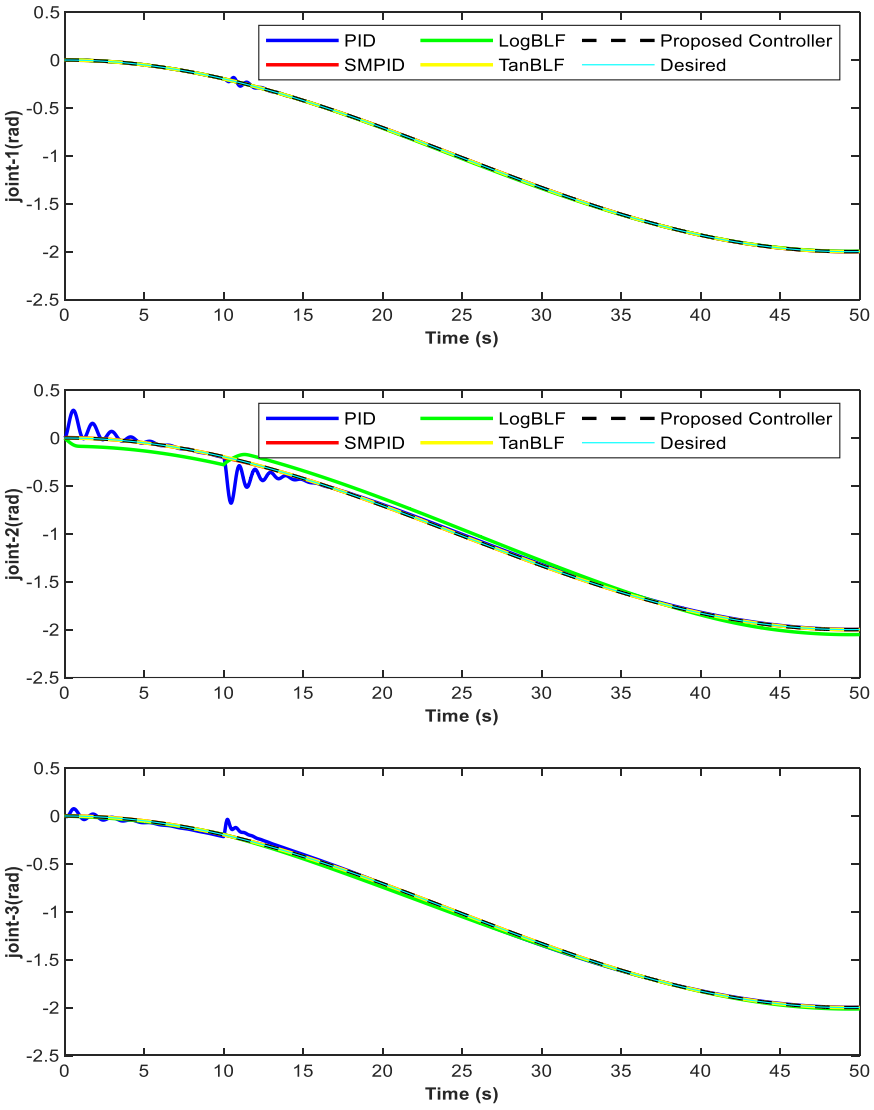

Fig. 21. Tracking performance with uncertainty in the inertia matrix.

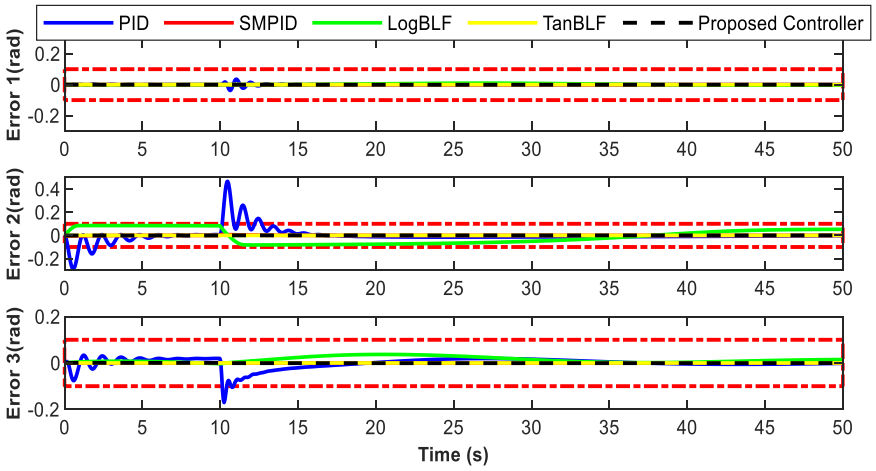

Fig. 22. Tracking error with uncertainty in the inertia matrix (Dashed red lines denote the PPB).

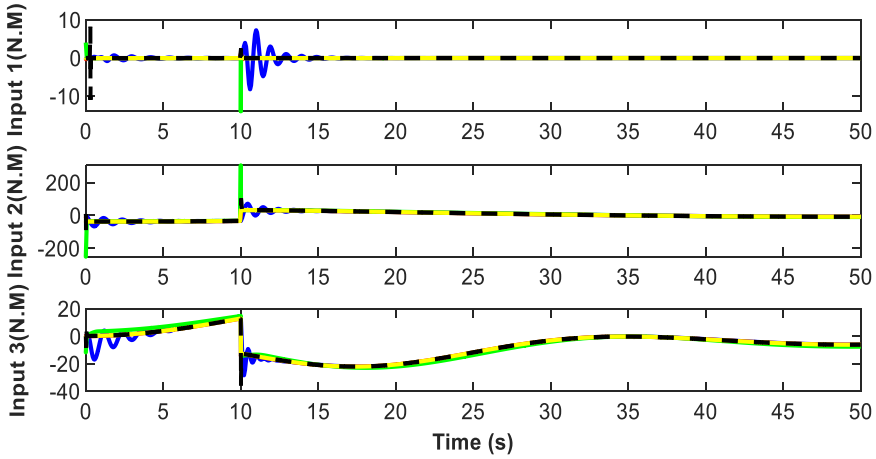

Fig. 23. The control signal with uncertainty in the inertia matrix.

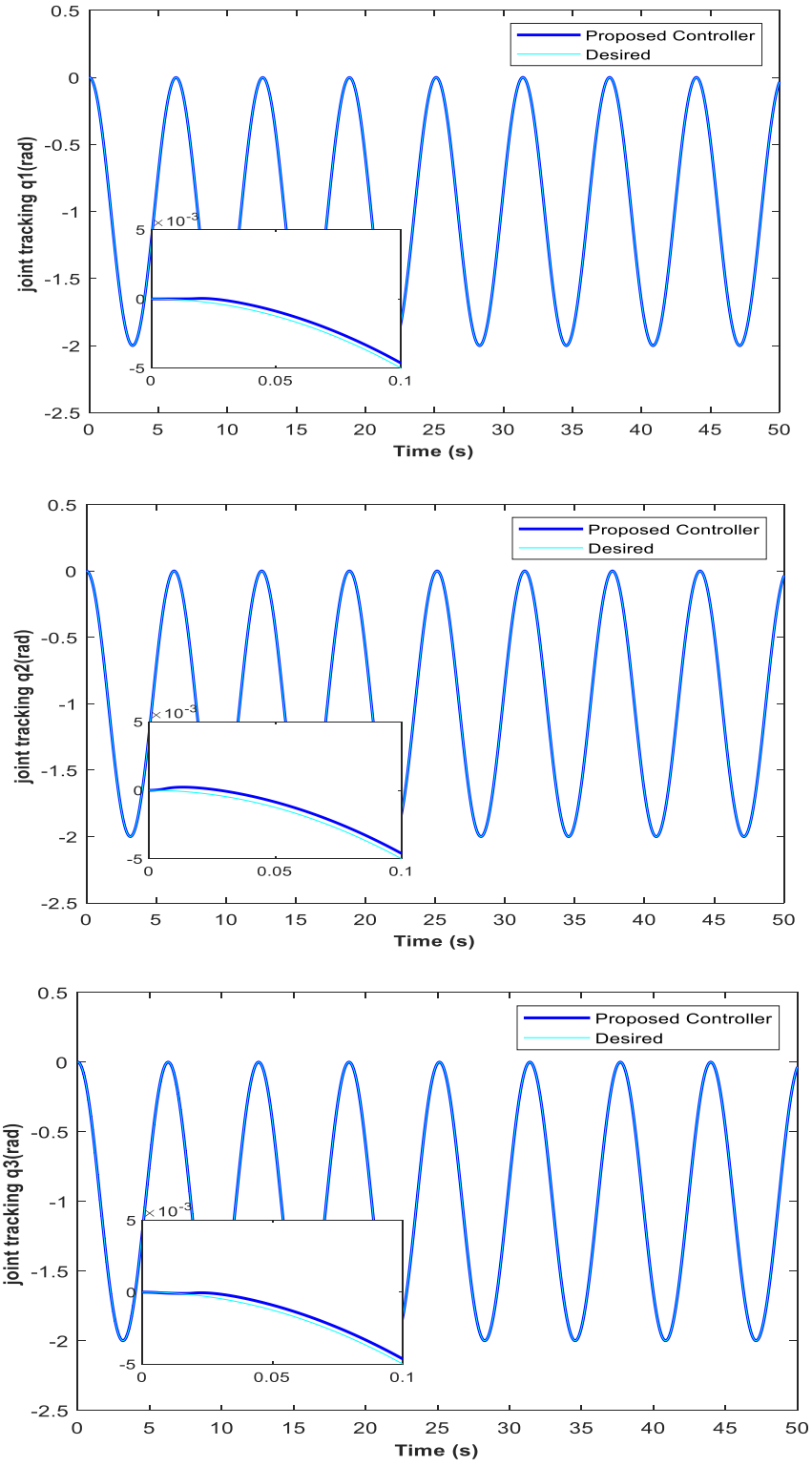

Fig. A- 1. Tracking performance in normal condition.

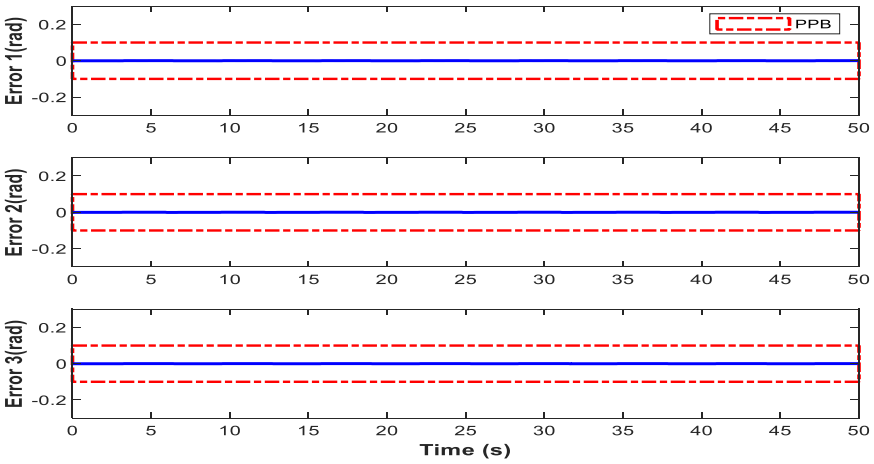

Fig. A-2. Tracking errors in normal condition (dashed red lines denote the PPB).

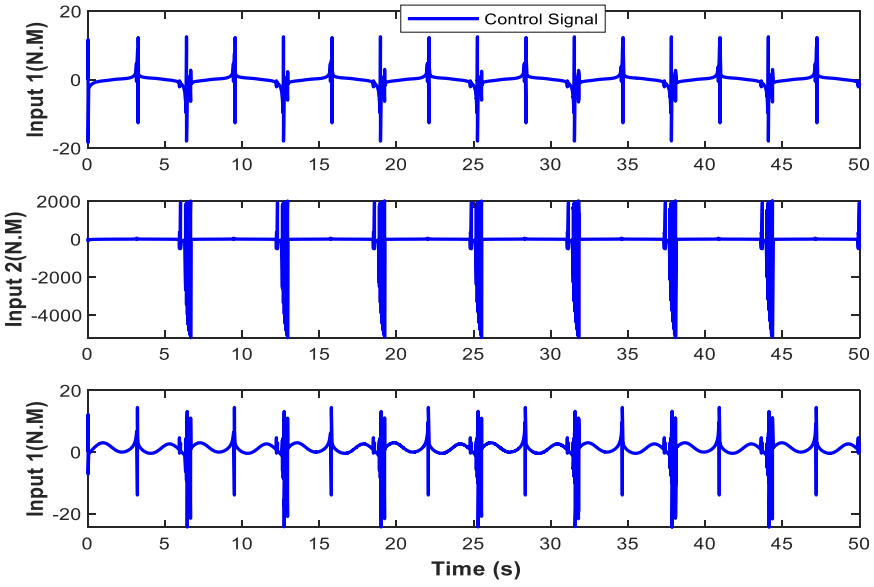

Fig. A-3. The control signal in normal condition.

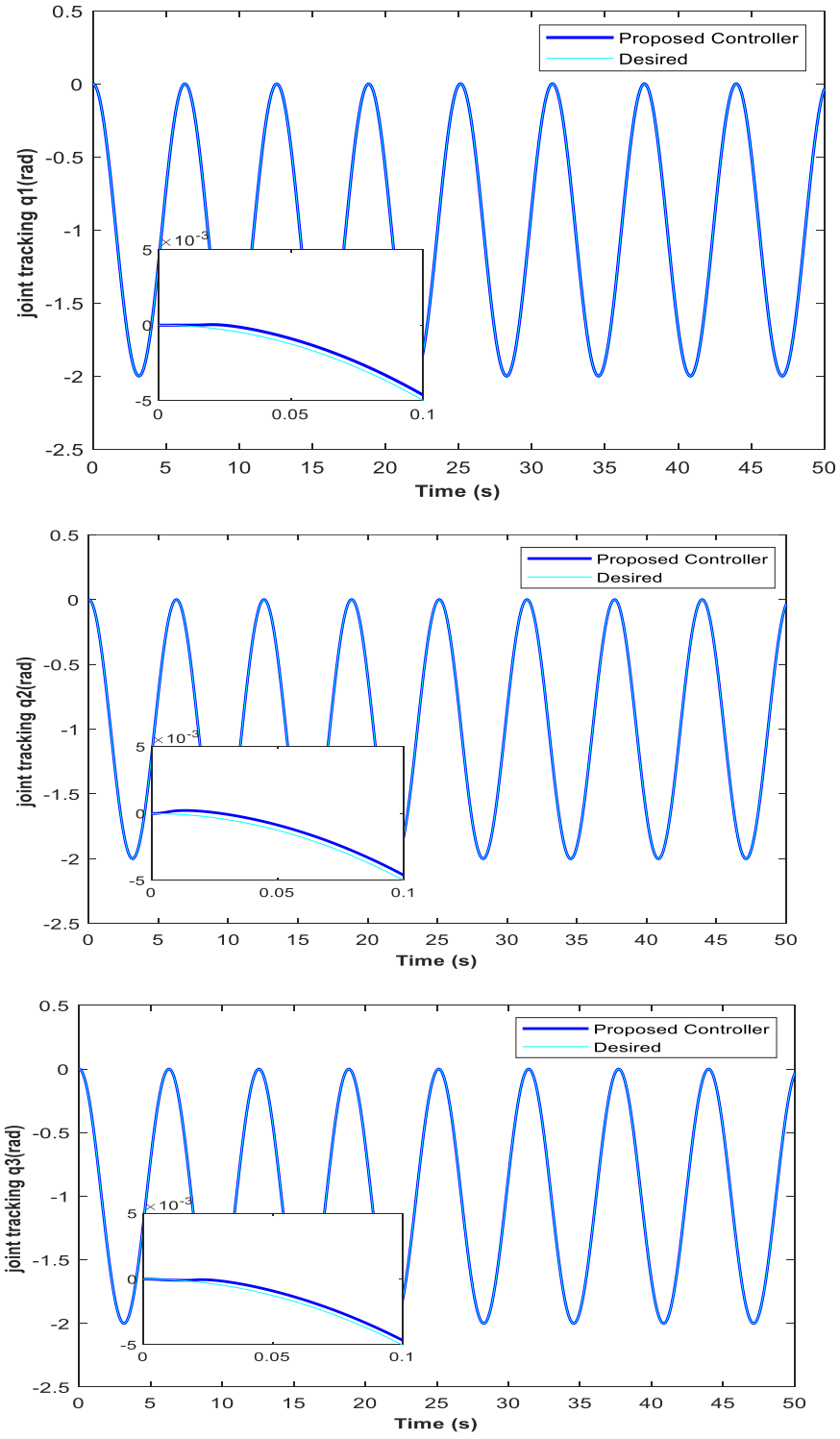

Fig. A-4. Tracking performance under actuator fault.

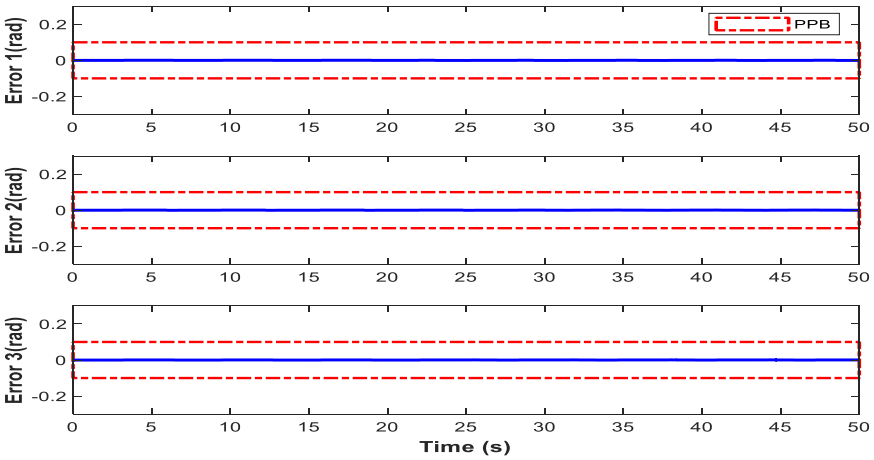

Fig. A-5. Tracking errors under actuator fault condition (dashed red lines denote the PPB).

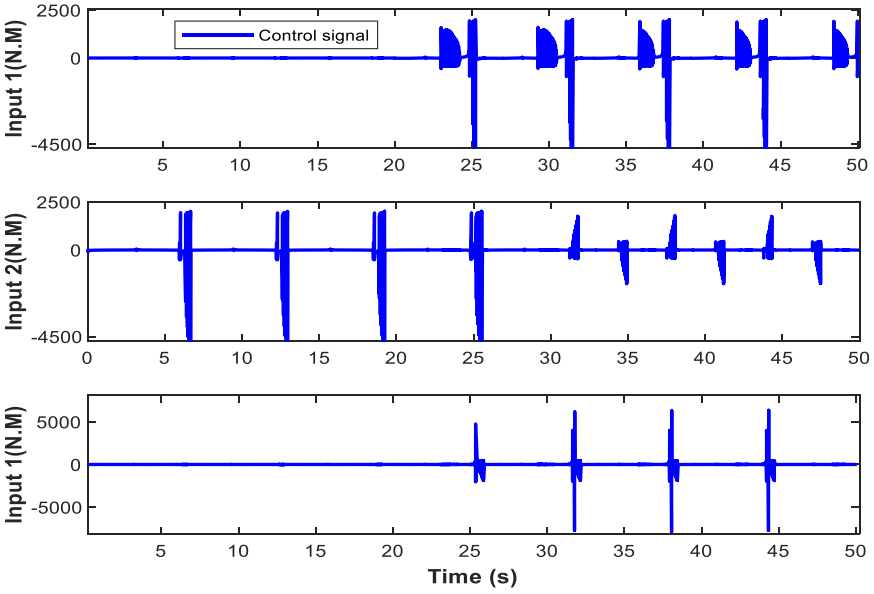

Fig. A-6. The control signal under actuator fault.

.

References

[1] Ahmed S, Wang H, Tian Y. Adaptive high-order terminal sliding mode control based on time delay estimation for the robotic manipulators with backlash hysteresis. IEEE Trans Syst Man Cybern Syst 2021;vol. 51(2):1128–37.

[2] Wang M, Yang A. Dynamic learning from adaptive neural control of robot manipulators with prescribed performance. EEE Trans Syst Man Cybern Syst 2017; vol. 47(8):2244–55.

[3] Habibi H, Yazdani A, Darouach M, Wang H, Fernando T, Howard I. Observer-based Sensor Fault Tolerant Control with Prescribed Tracking Performance for a Class of Nonlinear Systems. IEEE Trans Autom Control 2023. https://doi.org/10.1109/TAC.2023.3296494.

[4] Van M, Mavrovouniotis M, Ge SS. An adaptive backstepping nonsingular fast terminal sliding mode control for robust fault tolerant control of robot manipulators. IEEE Trans Syst Man Cybern Syst 2018;vol. 49(7):1448–58.

[5] Van M, Ceglarek D. Robust fault tolerant control of robot manipulators with global fixed-time convergence. J Frankl Inst 2021;vol. 358(1):699–722.

[6] He W, David AO, Yin Z, Sun C. Neural network control of a robotic manipulator with input deadzone and output constraint. IEEE Trans Syst Man Cybern Syst 2015; vol. 46(6):759–70.

[7] Song Y, Huang X, Wen C. Robust adaptive fault-tolerant PID control of MIMO nonlinear systems with unknown control direction. IEEE Trans Ind Electron 2017; vol. 64(6):4876–84.

[8] Ferrara A, Incremona GP. Design of an integral suboptimal second-order sliding mode controller for the robust motion control of robot manipulators. IEEE Trans Control Syst Technol 2015;vol. 23(6):2316–25.

[9] Bartolini G, Caputo W, Cecchi M, Ferrara A, Fridman L. Vibration damping in elastic robotic structures via sliding modes. J Robot Syst 1997;vol. 14(9):675–96.

[10] Raoufi M, Habibi H, Yazdani A, Wang H. Robust Prescribed Trajectory Tracking Control of a Robot Manipulator Using Adaptive Finite-Time Sliding Mode and Extreme Learning Machine Method. Robotics 2022;vol. 11(5):111.

[11] Asada H, Ma Z-D, Tokumaru H. Inverse dynamics of flexible robot arms: Modeling and computation for trajectory control. J Dyn Sys, Meas, Control 1990;vol. 112(2): 177–85.

[12] Zhang W, Han Q-L, Tang Y, Liu Y. Sampled-data control for a class of linear time-varying systems. Automatica 2019;vol. 103:126–34.

[13] Hong Y, Xu Y, Huang J. Finite-time control for robot manipulators. Syst Control Lett 2002;vol. 46(4):243–53.

[14] Lin F, Brandt RD. An optimal control approach to robust control of robot manipulators. IEEE Trans Robot Autom 1998;vol. 14(1):69–77.

[15] Yu J, Shi P, Liu J, Lin C. Neuroadaptive finite-time control for nonlinear MIMO systems with input constraint. IEEE Trans Cybern 2020.

[16] Li G, Yu J, Chen X. Adaptive fuzzy neural network command filtered impedance control of constrained robotic manipulators with disturbance observer. IEEE Trans Neural Netw Learn Syst 2021.

[17] He W, Ofosu Amoateng D, Yang C, Gong D. Adaptive neural network control of a robotic manipulator with unknown backlash-like hysteresis. IET Control Theory Appl 2017;vol. 11(4):567–75.

[18] Kim YH, Lewis FL. Optimal design of CMAC neural-network controller for robot manipulators. IEEE Trans Syst Man Cybern Syst 2000;vol. 30(1):22–31.
[19] He W, Dong Y, Sun C. Adaptive neural impedance control of a robotic manipulator with input saturation. IEEE Trans Syst Man Cybern Syst 2015;vol. 46(3):334–44.
[20] Keighobadi J, Xu B, Alfi A, Arabkoohsar A, Nazmara G. Compound FAT-based prespecified performance learning control of robotic manipulators with actuator dynamics. ISAT 2022;vol. 131:246–63.
[21] He W, Dong Y. Adaptive fuzzy neural network control for a constrained robot using impedance learning. IEEE Trans Neural Netw Learn Syst 2017;vol. 29(4):1174–86.
[22] Van M, Ge SS, Ren H. Finite time fault tolerant control for robot manipulators using time delay estimation and continuous nonsingular fast terminal sliding mode control. IEEE Trans Cybern 2016;vol. 47(7):1681–93.
[23] Ferrara A, Incremona GP, Cucuzzella M. SIAM. Adv Optim Based sliding mode Control: Theory Appl 2019.
[24] Tang Y. Terminal sliding mode control for rigid robots. Automatica 1998;vol. 34 (1):51–6.
[25] Zhihong M, Paplinski AP, Wu HR. A robust MIMO terminal sliding mode control scheme for rigid robotic manipulators. IEEE Trans Autom Contr 1994;vol. 39(12): 2464–9.
[26] Feng Y, Yu X, Man Z. Non-singular terminal sliding mode control of rigid manipulators. Automatica 2002;vol. 38(12):2159–67.
[27] Yu S, Yu X, Shirinzadeh B, Man Z. Continuous finite-time control for robotic manipulators with terminal sliding mode. Automatica 2005;vol. 41(11):1957–64.
[28] Galicki M. Finite-time control of robotic manipulators. Automatica 2015;vol. 51: 49–54.
[29] Meng F, Zhao L, Yu J. Backstepping based adaptive finite-time tracking control of manipulator systems with uncertain parameters and unknown backlash. J Frankl Inst 2020;vol. 357(16):11281–97.
[30] Song Y, Huang X, Wen C. Robust adaptive fault-tolerant PID control of MIMO nonlinear systems with unknown control direction. IEEE Trans Ind Electron 2017; vol. 64(6):4876–84.
[31] Meng F, Zhao L, Yu J. Backstepping based adaptive finite-time tracking control of manipulator systems with uncertain parameters and unknown backlash. J Frankl Inst 2020;vol. 357(16):11281–97.
[32] Fan Y, Kang T, Wang W, Yang C. Neural adaptive global stability control for robot manipulators with time-varying output constraints. Int J Robust Nonlinear Control 2019;vol. 29(16):5765–80.
[33] Lu S-M, Li D-P, Liu Y-J. Adaptive neural network control for uncertain time-varying state constrained robotics systems. I*EEE Trans Syst Man Cybern Syst* 2017;vol. 49 (12):2511–8.
[34] Sun W, Wu Y, Lv X. Adaptive Neural Network Control for Full-State Constrained Robotic Manipulator With Actuator Saturation and Time-Varying Delays. IEEE Trans Neural Netw Learn Syst 2021:1–12.
[35] Yu X, He W, Li H, Sun J. Adaptive fuzzy full-state and output-feedback control for uncertain robots with output constraint. I*EEE Trans Syst Man Cybern Syst* 2020: 1–14.
[36] Zhai J, Xu G. A novel non-singular terminal sliding mode trajectory tracking control for robotic manipulators. IEEE Trans Circuits Syst II Express Briefs 2020; vol. 68(1):391–5.
[37] Van M, Ge SS, Ren H. Finite time fault tolerant control for robot manipulators using time delay estimation and continuous nonsingular fast terminal sliding mode control. IEEE Trans Cybern 2016;vol. 47(7):1681–93.
[38] Cui Q, Cao H, Wang Y, Song Y. Prescribed time tracking control of constrained Euler–Lagrange systems: An adaptive proportional–integral solution. Int J Robust Nonlinear Control 2021.
[39] Song Y, Huang X, Wen C. Tracking control for a class of unknown nonsquare MIMO nonaffine systems: A deep-rooted information based robust adaptive approach. IEEE Trans Autom Control 2016;vol. 61(10):3227–33.
[40] Krstic M, Deng H. Stabilization of Nonlinear Uncertain Systems. Springer,; 1998.
[41] Cui Q, Cao H, Wang Y, Song Y. Prescribed time tracking control of constrained Euler–Lagrange systems: An adaptive proportional–integral solution. Int J Robust Nonlinear Control 2021:1–19.
[42] H.-C. Lin, T.-C. Lin, and K. Yae, On the skew-symmetric property of the Newton-Euler formulation for open-chain robot manipulators, in Proceedings of 1995 American Control Conference-ACC'95, 1995, vol. 3: IEEE, pp. 2322–2326.
[43] Song Y-D, Zhou S. Tracking control of uncertain nonlinear systems with deferred asymmetric time-varying full state constraints. Automatica 2018;vol. 98:314–22.
[44] B. Armstrong, O. Khatib, and J. Burdick, The explicit dynamic model and inertial parameters of the PUMA 560 arm, in Proc. IEEE Int. Conf. Robotic Auto., 1986, vol. 3: IEEE, pp. 510–518.
[45] Van M, Mavrovouniotis M, Ge SS. An adaptive backstepping nonsingular fast terminal sliding mode control for robust fault tolerant control of robot manipulators. IEEE Trans Syst, Man, Cyber: Syst 2018;vol. 49(7):1448–58.
[46] Su Y, Müller PC, Zheng C. Global asymptotic saturated PID control for robot manipulators. IEEE Trans Control Syst Technol 2009;vol. 18(6):1280–8.
[47] Amer AF, Sallam EA, Elawady WM. Adaptive fuzzy sliding mode control using supervisory fuzzy control for 3 DOF planar robot manipulators. Appl Soft Comput 2011;vol. 11(8):4943–53.
[48] Yang C, Huang D, He W, Cheng L. Neural control of robot manipulators with trajectory tracking constraints and input saturation. IEEE Trans Neural Netw Learn Syst 2021;vol. 32(9):4231–42.
[49] Ghanooni P, Habibi H, Yazdani A, Wang H, MahmoudZadeh S, Mahmoudi A. Rapid detection of small faults and oscillations in synchronous generator systems using GMDH neural networks and high-gain observers. Electronics 2021;vol. 10(21): 2637.
[50] Chen T, Wang C, Hill DJ. Small oscillation fault detection for a class of nonlinear systems with output measurements using deterministic learning. Syst Control Lett 2015;vol. 79:39–46.
[51] Nigam R, Lee C. A multiprocessor-based controller for the control of mechanical manipulators. IEEE J Robot Autom 1985;vol. 1(4):173–82.